Origin of the variation of amplitude of the Hawaiian swell

Chris Weller

GEOL 394

21 November 2012

Dr. Laurent Montesi

Contents

Abstract

A swell of debated origin has formed around the Hawaiian island chain. The amplitude of the swell is more significant along the sides than to the head of the chain to the southeast. Measurements have shown that the height of the swell to the northeast and southwest of the chain is as much as four times larger than at the head of the island chain. One hypothesis for the origin of the swell is linked to flexure of the oceanic plate caused by the weight of basaltic accumulation. Analytical models show that the deflection induced by a load on an elastic plate causes upward displacement some distance from the load. Accordingly, the model of a truncated line load shows a greater bulge size along the sides of the load than at the head where the line is truncated in agreement with observations of the Hawaiian island. Alternatively, the swell may be related to buoyancy and heat transferred to the lithosphere from the hot spot beneath Hawaii. The heat from the hot spot causes the mantle to become less dense and more buoyant, producing an upward deflection of the plate. The amplitude of the swell is less significant to the southeast because the hot spot is deflected to the northwest due to the plate motion. The models shows distribution of heat as well as the velocity and direction of fluid flow as the plume rises. The plume model is based on the Stokes equation that describe momentum balance in a fluid and the heat equation considering both heat advection and diffusion. The increased buoyancy centered over the head of plume produces normal stresses at the surface of the model that will be balanced by topography. A 3D model including motion of the surface plate shows variation in swell amplitude but is dissimilar to the variation in amplitude around the Hawaiian island chain.

1 Introduction

Swells are defined as a rounded elevation. Swells are important in determining if hot spot volcanism is due to upwelling of plumes from the deep mantle (DeLaughter et. al. 2005). A well defined swell is present around the Hawaiian Islands (Figure 1). The significance of the swell can be seen in the red coloration along the sides of the island chain. According to Zhong and Watts (2002) the swell is 1000 km wide and 1.5 km high along the side of the island chain. The amplitude of the swell gradually diminishes as it curves around the head of the island chain to the southeast.

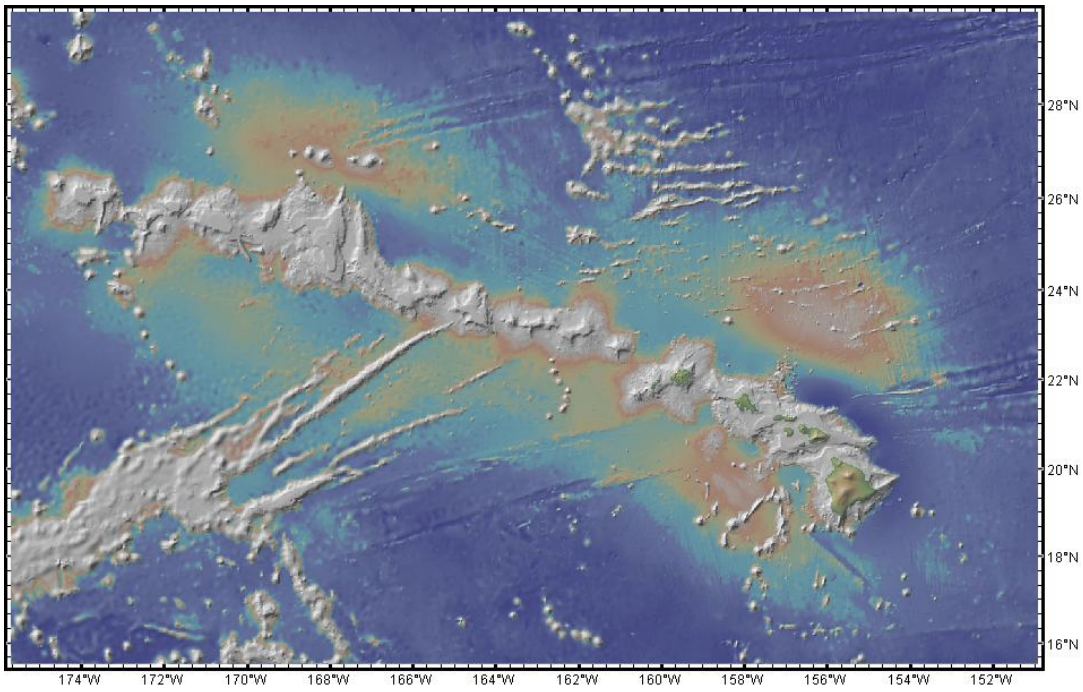

Figure 1. An image showing the topography of the Hawaiian Island chain. The red coloration indicates topographical change in the positive z direction (coming out of the page). The gray coloration to the southwest indicates basalt deposits.

Surrounding the Hawaiian island chain is a topographical swell, the cause of which, has yet to be determined. Such swells can be seen around many oceanic islands (DeLaughter et. al. 2005). However, the swell around the Hawaiian island chain is anomalous. The Hawaiian swell is most significant along the sides of the island chain. Zhong and Watts (2002) hypothesized that the formation of the swell is due to flexure caused by the emplacement of basaltic magma above. The added weight of the island due to magma emplacement the crust and mantle beneath to flex under the added weight. Alternatively, the swell can be the result of heat transfer from an anomalous hot spot beneath the island chain. Zhong and Watts (2002) also hypothesized that heat transfer and buoyancy forces from the hot spot beneath Hawaii are also responsible for the magnitude of the swell. Because the hot spot is hotter than the surrounding mantle, the lithosphere in contact with the hot spot is hotter than the reference oceanic lithosphere. This causes the crust to be less dense and isostasy allows it to float higher than the surrounding crust. The amplitude of the swell is less significant to the southeast because the hot spot is deflected to the northwest due to the plate motion.

in this study, I examined the significance of these both flexure and hot spot heat transfer, and their effect on the amplitude of the swell. First, I analyzed the variations in the amplitude of the swell around the Hawaiian island. Then, I generated various models mimicking the flexural processes, as well as the plume heat transfer, occurring beneath the Hawaiian Island chain coupled with plate motion.

1.1 1.1 Formation of Seamounts and Island Chains

According to Watts (2001), seamounts and oceanic islands are formed in a variety of tectonic settings, including mid-ocean ridges (MOR) and transform boundaries. However, many seamounts and oceanic islands are found in the interior of oceanic plates, particularly the Western Pacific (Watts, 2001). These are believed to be the result of mantle hot spots breaching through the thin lithosphere, causing volcanic activity throughout the interior of the plate.

Oceanic island volcanoes are made of basaltic lava flows. As the lava breaches the surface, it solidifies and forms the base for the next flow. The bases build on each other, forming the seamounts and oceanic islands. This formation is known as summit eruption seen in the Figure 2. As this occurs the crust and mantle below bend under the added weight of the deposit.

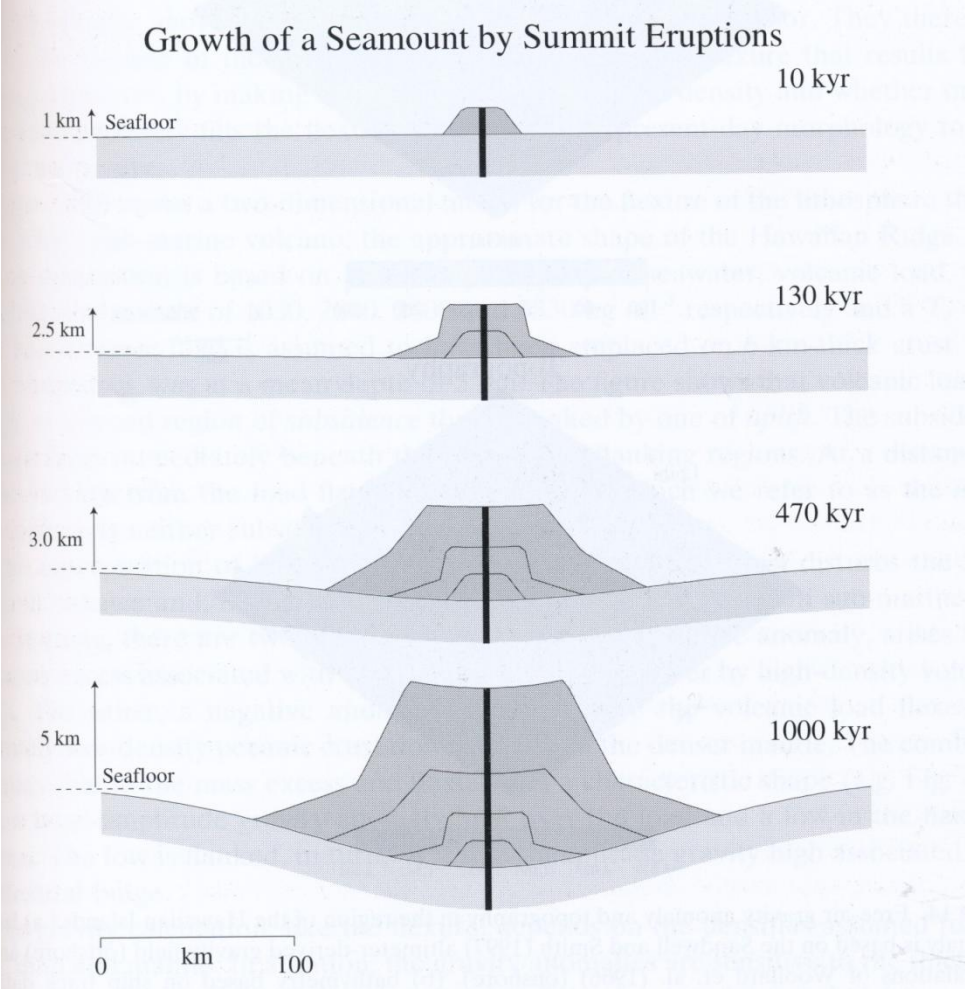

Figure 2. Image provided by Watts (2001), a model of seamount growth by summit eruption. Ages are derived from the eruption rates and time-scale of stress relaxation in the oceanic lithosphere.

The growth rate of seamounts has been determined to be relatively fast. According to Watts (2001), the eruption rates of Hawaii are 0.050 km^3yr^{-1}. Watts (2001) also states that the total volume of the Hawaiian island is $1.1x10^5$ km^3. This volume of material causes the crust and mantle beneath to subside under the weight.

According to Wilson (1963), the ages of the islands increase traveling along the chain. suggesting that the islands form as the plate is pushed over a hotspot. Over time, the point where the hotspot breeches the surface moves due to plate tectonics. The hot spot must then breech the lithosphere again and begins forming a new island through summit eruption at a new coordinate on the plate.

2 Bathymetry

Using GeoMapApp a program which provides topographical information for nearly the entire surface of the Earth, a topographical image of the Hawaiian island chain was obtained. (GeoMapApp is a program provided by the Marine Geoscience Data System.) The bathymetric grid for the region surrounding the Hawaiian islands obtained using GeoMapApp was then downloaded into the program Fledermaus (Figure 1). Fledermaus is 3D visualization software used to obtain topographic and bathymetric data. This software allows for the creation and interaction full-resolution terrain and bathymetric surface models. Looking at Figure 1 the swell along the side of the island appears to be more significant than at the head of the island, to the southeast.

2.1 Bathymetric Profiles

Using Fledermaus, ten bathymetric profiles around the head of the island were taken (Figure 3a-c and Appendix A). Four profiles were taken of the swell, along the northeast side of the island chain (Figure 3a and Appendix A). Another three profiles were taken one the opposing side swell to the southwest of the island chain (Figure 3c and Appendix A). Finally, three profiles were taken at the head of the island chain, measuring the lesser swell to the southeast (Figure 3b). All three profiles, measuring the swell to the southeast, radiated outward from a single point, which can be seen in figure 3b, from the Island of Hawaii.

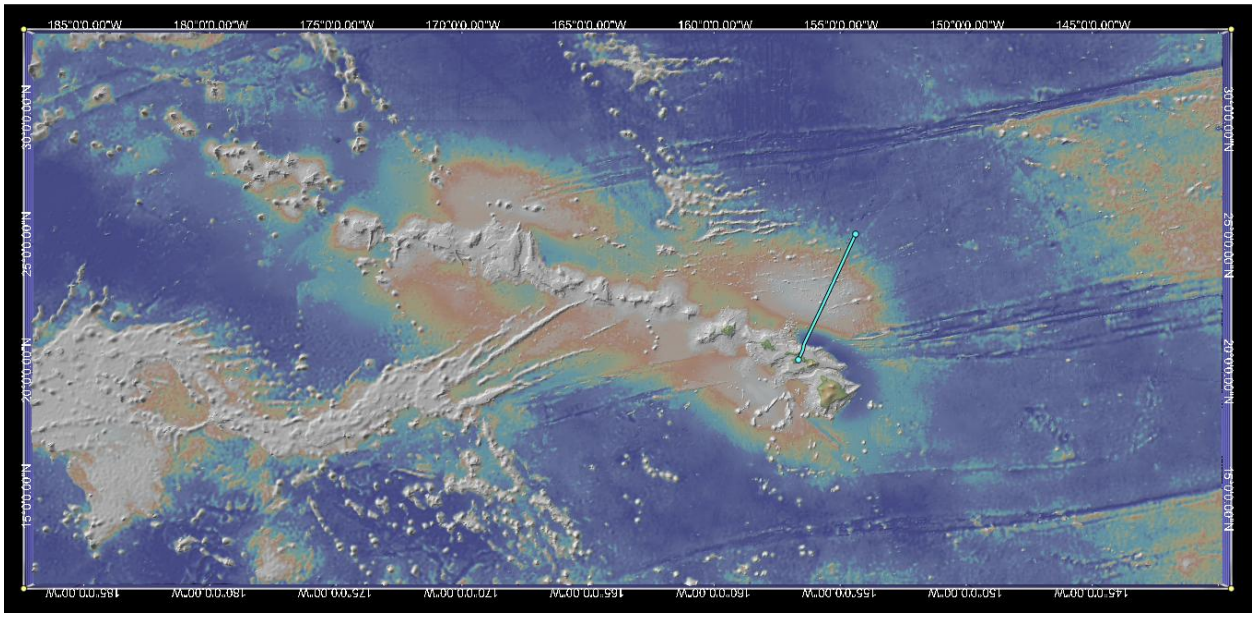

Figure 1a Topographical image showing the line for bathymetric profile in Figure 4a.

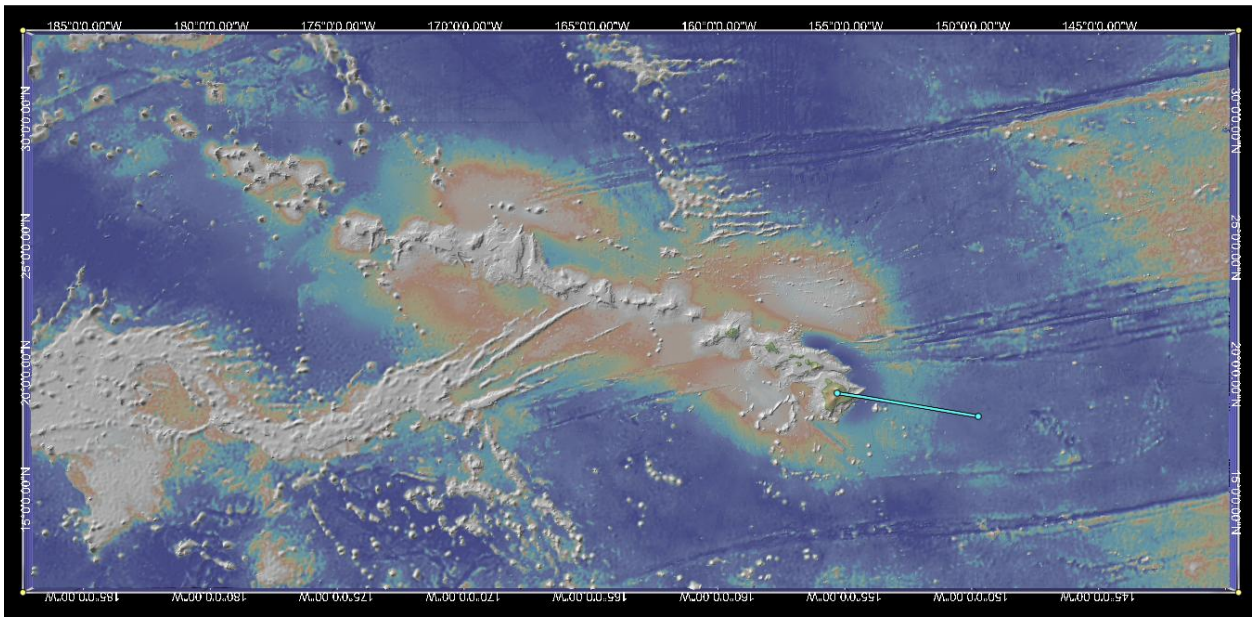

Figure 2b Topographical image showing the line for bathymetrical profile in Figure 4b.

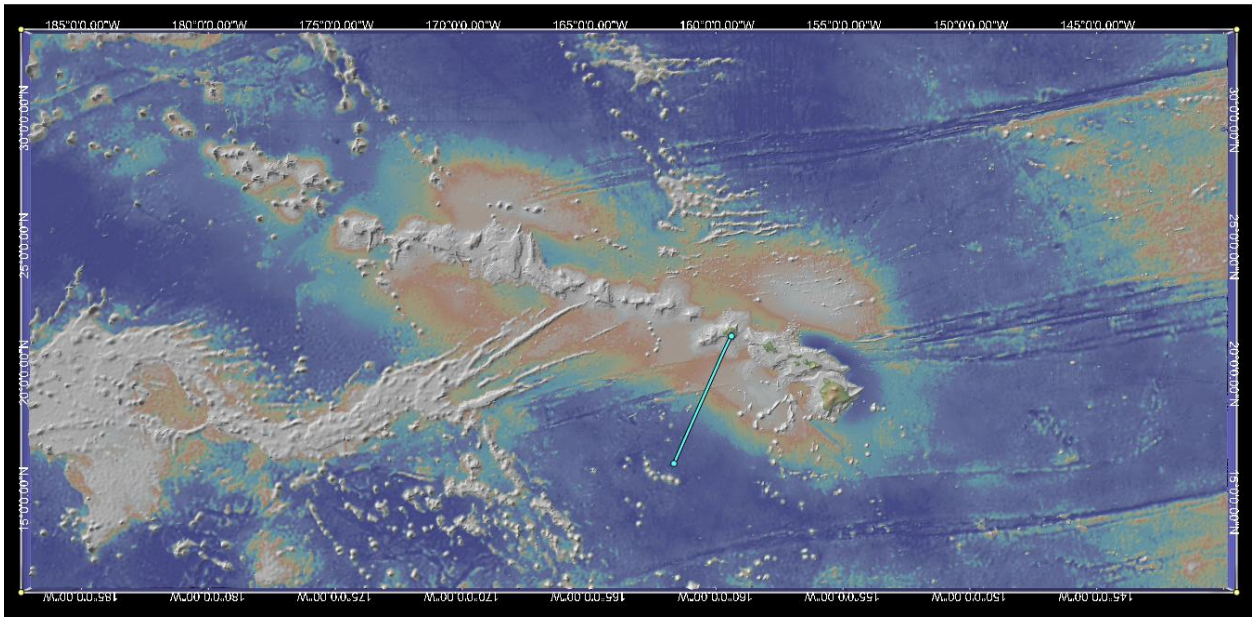

Figure 3c Topographical profile showing the line of the bathymetrical profile in Figure 4c.

The bathymetric profiles in Figures 4a-c correspond to the profile cuts shown in Figures 3a-c. The amplitude of the swell is noticeably larger in the profiles taken to the northeast and southwest of the island chain (Figure 4a and 4c). Ignoring the smaller seamount formation on the swells, the northwest swell has an approximate amplitude of 1200 m. The swell to the southwest has a slightly smaller amplitude of 1000 m. However, the size of these swells is still significantly larger than the swell to the southeast of the island chain, whose amplitude is approximately 300 m (Figure 4b). The profiles indicate that the swell at the head of the island is approximately 25-30% the amplitude the swell along the side of the island chain. The other bathymetric profile can be seen in Appendix B.

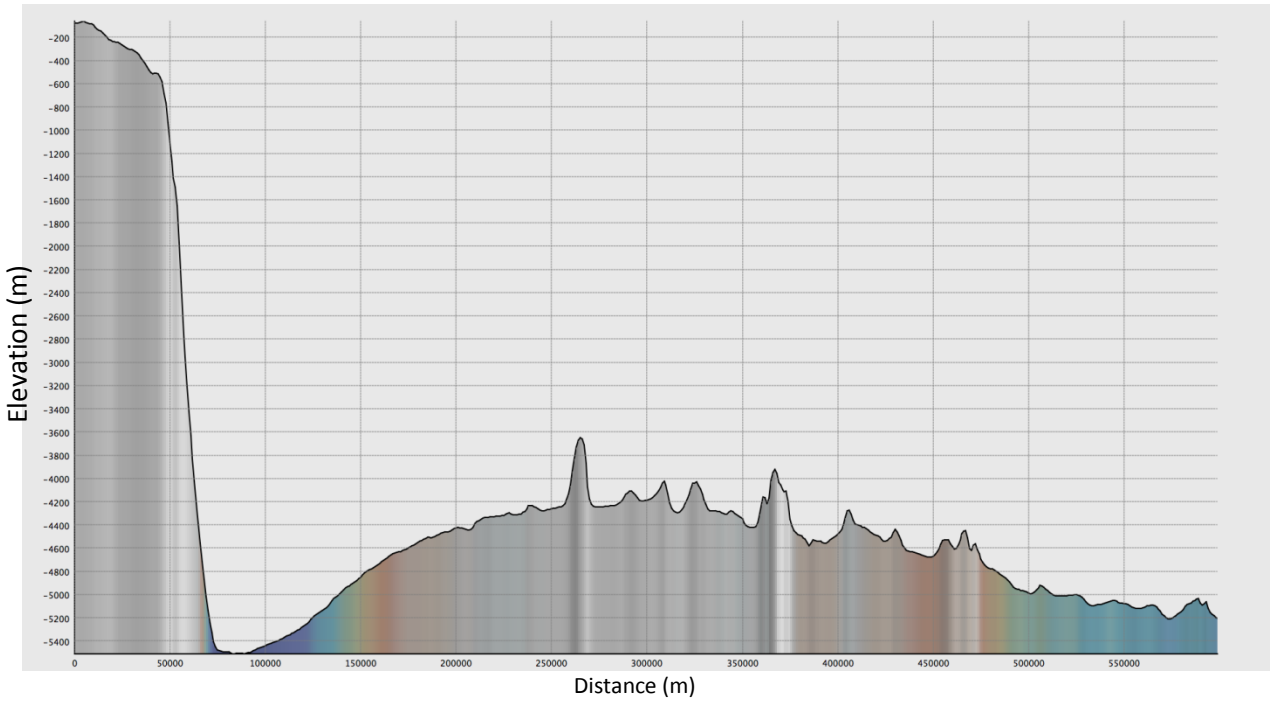

Figure 4a. Bathymetric profile of the swell to the northeast of the Hawaiian Island. Location shown in Figure 3a.

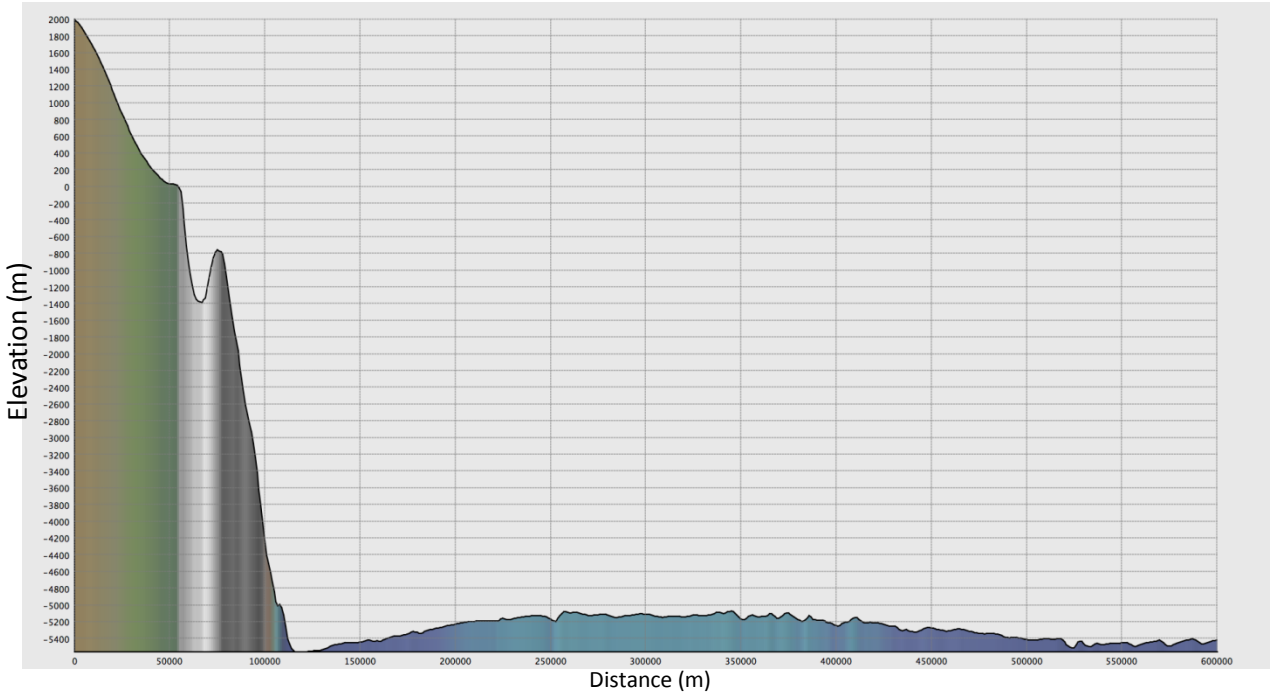

Figure 4b. Bathymetric profile of the swell to the head (southeast) of the Hawaiian Island. Location shown in Figure 3b.

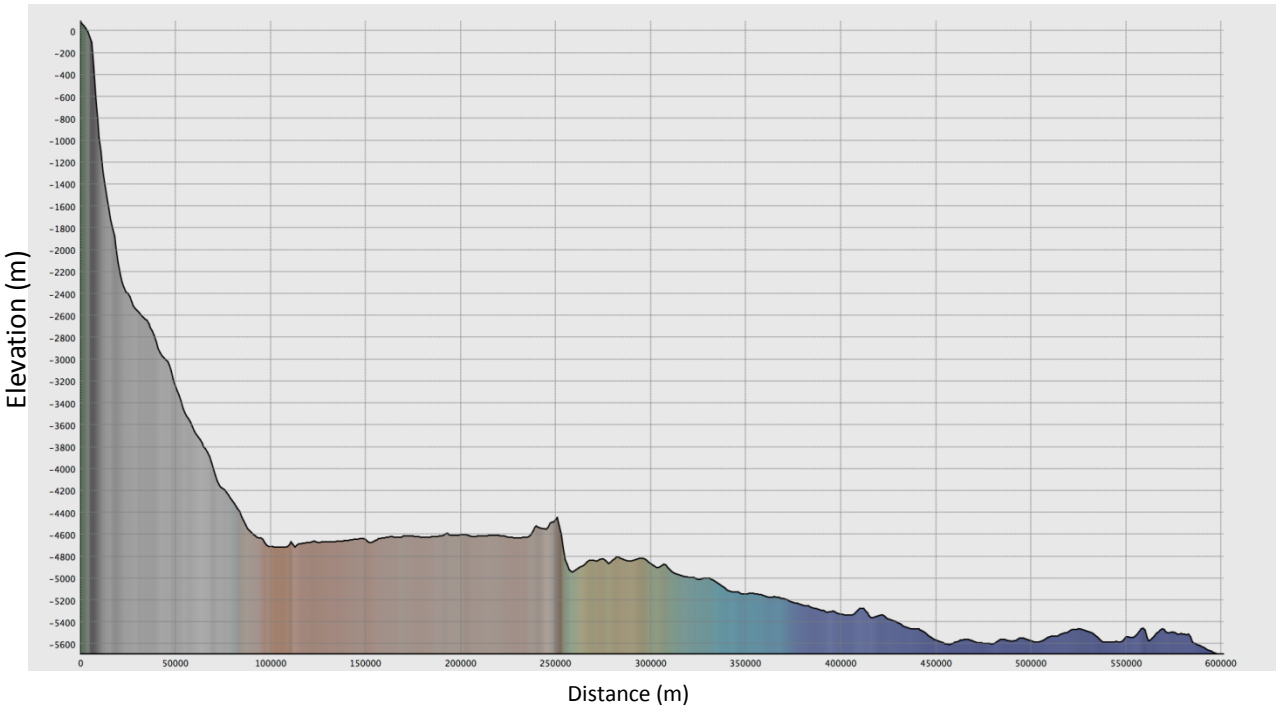

Figure 4c Bathymetric profile of the swell to the southwest of the Hawaiian Island. Location shown in Figure 3c.

3 Flexure

Turcotte and Schubert (2002) defines flexure as "the bending of the lithosphere to known surface load." This definition describes what is happening to the plate beneath the Hawaiian Islands. As basalts accumulate from summit eruptions, the weight causes the crust and mantle below the Hawaiian Islands to be displaced.

3.1 Equations of Flexure

The general equation for the deflection of an elastic shell is given by:

Equation 1. $$D\nabla^4 w + D\beta^{-4} w = q$$

where D is the flexural rigidity, β is the flexural parameter, w is the vertical deflection of the plate, and q is the load (Brotchie and Silvester 1969). D $\nabla^4 w$ represents bending moments of the elastic plates. $D\beta^{-4} w$ is the hydrostatic restoring force due the difference in density between the materials above and below the plate. The load given by q, is the deposition of the Hawaiian Island.

D and β are defined as:

Equation 2. $$D = \frac{EH^3}{12(1-\nu^2)}$$

Equation 3. $$\beta = \left[\frac{D}{(\rho_m - \rho_{infill})g}\right]^{1/4}$$

where E is Young's Modulus; ν is Poisson's ratio; H is the thickness of the plate; ρ_m and ρ_{infill} are the densities of the mantle below and the sediment and water above the plate; and g is the acceleration of gravity. The value of these parameters are given in Table 1.

Quantity	Symbol	Value	Units
Young' s modulus	E	70	GPa
Poisson's ratio	v	0.25	
Thickness of the Plate	H	50	km
Density of Mantle	ρ_m, ρ_o	3300	kgm^{-3}
Density of Water and Sediment	ρ_{infill}	1000	kgm^{-3}
Flexural Rigidity	D	$7.78x10^{23}$	Nm
Flexural Parameter	β	7.63x10	kgm^2
Acceleration of Gravity	g	10	ms^{-2}
Coefficient of Thermal Conductivity	α	$3.5x10^{-5}$	K^{-1}
Heat Conductivity	*k*	4.125	$kgm^{-1}s^{-1}$
Heat Capacity of Fluid	C_p	1250	J/Kg
Thermal Diffusivity	κ	$1.0x10^{-6}$	m^2s^{-1}
Initial Temperature	T_0	200	K
Vertical Displacement	w	200	km

Table 1.The values in this table were drawn from multiple sources primarily Watts, 2001; Davies, 1991; Turcotte and Schubert 2002.

Analytical solutions are available for simple load geometry such as a line load or a point load (Watts 2001). For more complicated cases it is possible to find numerical solutions for these equations described the two analytical solutions. These are also present preliminary numerical solutions obtained through the Finite Elements Method.

3.2 Analytical solution

3.2.1 Line Load

In the presence of a line load, parallel to the y-axis, the solution should be invariant with respect to y and symmetric with respect to x. Equation 1 simplifies to:

Equation 4. $$\frac{d^4w}{dx^4} + \beta^{-4}w = \frac{q}{D}$$

Its solution is:

Equation 5. $$w = w_0 e^{-\lambda x}[cos\lambda x + sin\lambda x]$$

Where w_0 is defined as the amplitude of deflection. The flexural wavelength, λ controls the wavelength of the deformation given by:

Equation 6. $$\lambda = \frac{\sqrt{2}}{\beta}$$

Figure 5 represents the graph of the solution (Equation 5). The blue line indicates the profile of deflection for a line load. The points where w/w0 is greater than zero represents bulging or swelling of crust due the displacement caused by the load.

3.2.2 Point Load

In the presence of a point load at (0,0), the solution should be axisymmetric meaning it is symmetrical along a defined axis, in this case the z-axis. The solution depends only on r, the distance from the point and is given by:

Equation 7. $$w = w_k kei\left(\frac{r}{\beta}\right)$$

Here $w_k = w_0/kei(0)$. Kei is the imaginary part of the modified Bessel function of the second kind, a special mathematical function that is used to express analytical solutions to many axisymmetric problems in physics [Abramowitz and Stegun, 1972]. Using MATLAB I built a look up table to define kei, according to the values obtained using a Kelvin function calculator on the website Keisan.com (Appendix C).

The solution to the axisymmetric flexure problem is represented by the red line in Figure 5. Considering the same deflection at the source, the swell due to a point load is clearly less significant than the swell caused by a line load (Figure 5). Therefore, we can pose a first hypothesis:

Hypothesis 1: *The smaller amplitude of the Hawaiian swell to the southeast of the islands compared to the sides of the chain is due to different geometry of the flexural response: 2D response along the side, axisymmetric to the southeast of the chain.*

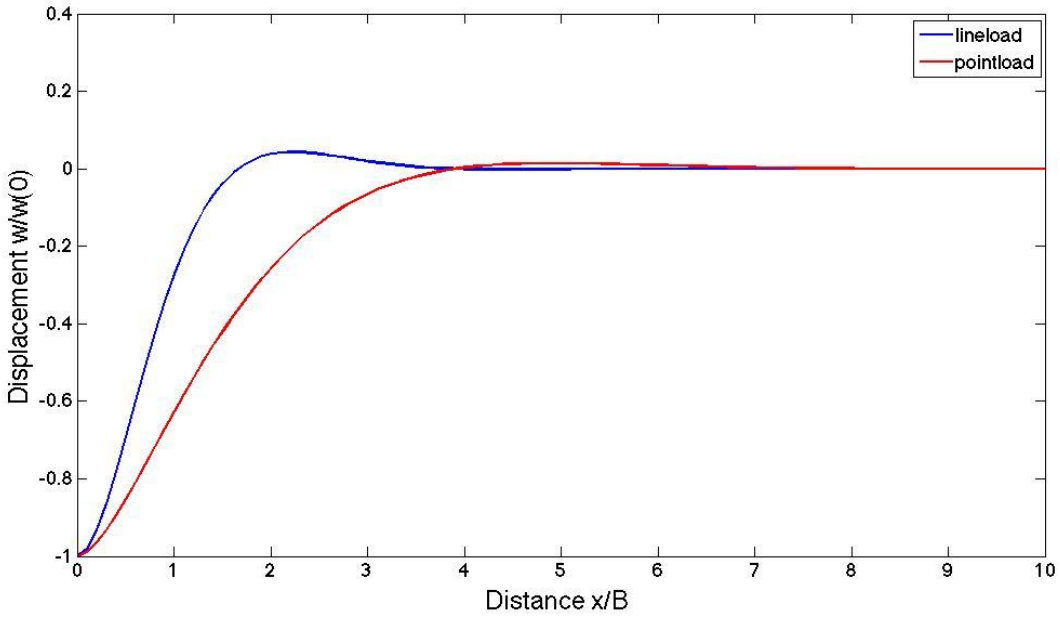

Figure 5. Graph of equations 4 (blue) and equation 5 (red) generated in MATLAB. MATLAB code for graph provided in Appendix D.

3.3 Numerical model

COMSOL Multiphysics® is a modeling software that solves sets of partial differential equations representing physical processes such as heat diffusion and advection, mantle flow, and elastic flexure, using the Finite Element Method. The software is used extensively in Dr. Montesi's group (e.g. Mitchell et al., 2011; Montési et al., 2011). The Finite Element methods break the physical space over which a solution is sought into a collection of objects of simple geometry or elements. The solution is parameterized by values of physical quantities at a few nodes related to these elements. This makes it possible to obtain solutions of physical problems in regions with complex geometries, or in our case, complex load geometry.

3.3.1 Model setup

The models shown in Figures 6-8 illustrate the flexure obtained for loads of various geometry. The model geometry is first defined by a two dimensional work plane. This work plane rests upon the xy-plane, with the center of the plane at x = 0 m for all of y. The axes in Figures 6-8 are defined as; x, going back into the right; y, going back into the left; and z, perpendicularly intersecting the x and y axes.

Each model represents a different flexural event caused by a different load. The first, in Figure 6, represents an infinite line load. Figure 7 is the flexural event caused by a singular point load. Finally, Figure 8 represents the flexural event of a truncated line load. The physics of these models was described in Section 3.1 given by Equation 1. The solution for a line load was presented in Section 3.2.1, given by Equation 5. The physics of the point load are defined in Section 3.2.2 given by Equation 7.

The edges of models in Figure 6-8, at x = -750 km, x = 750 km and y = 1,500 km, are given a prescribed displacement of zero, in the z direction. This means that they do not move under the influence of the loads placed on the models. The entire surface of the model is also given a face load pushing in the positive z direction. This face load acts as the buoyant hotspot beneath pushing up against the underside of the crust.

The discretization of the computation domain is defined as a mesh laid over the surface of the plane. The mesh provides the points where data is collected. The finer the triangular matrix of the mesh, the more points of data there are to collect and the more reliable the solution. However, low resolution is acceptable far from the loads. The mesh is defined as having a very fine matrix along the edges of displacement and symmetry, which gradually gets coarser extending out over the work plane.

Finally, the last boundary condition set within the models is defined symmetry. All the models presented have defined symmetry which will be described in the discussion of each model.

3.3.2 Flexure Models of Given Displacement

COMSOL models were generated represent the flexural occurrences at the Hawaiian Island chain. Various loads will be defined atop a plane formatted to represent the Earth's crust. Figures 6-8 represent the different loads the Hawaiian Islands are placing on the crust beneath.

Figure 6 represents a line load. The load itself is given a prescribed displacement of 8000 m in the negative z direction along the x = 0 m axis. This displacement is represented by the dark red coloration. The displacement caused by the load produces bulges of 287 m in the positive z direction, represented by the dark blue coloration.

The boundary conditions of this model slightly vary compared to the other two models. The described displacement of 0 m only applies to the edges parallel to the y axis in this model. This is because the displacement needs to affect the edges perpendicular to the y axis. Another boundary condition set in this model is the symmetry through the center at x = 0 m for all of y. This allows the amplitude of the bulge to be identical on either side of the load.

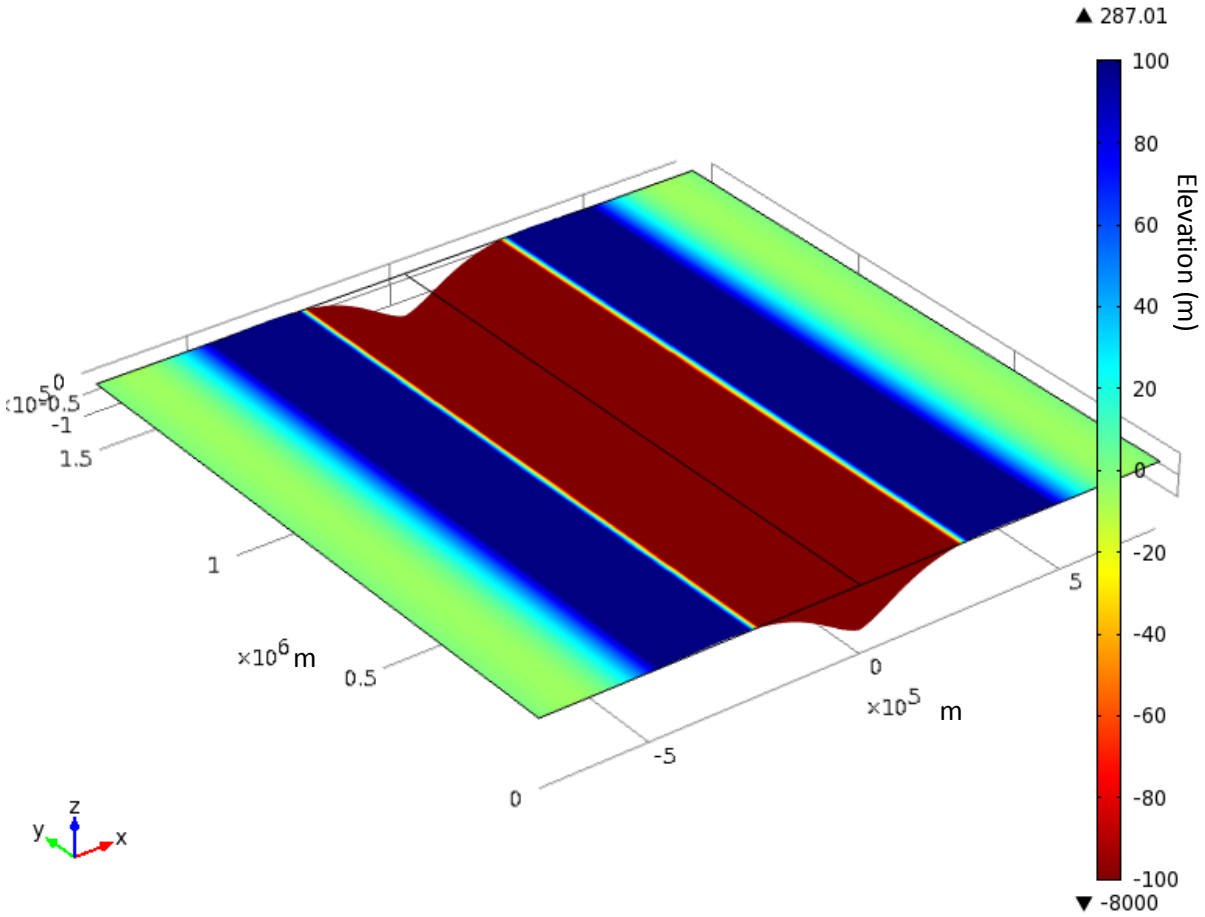

Figure 6 Numerical model of a line load with a given displacement.

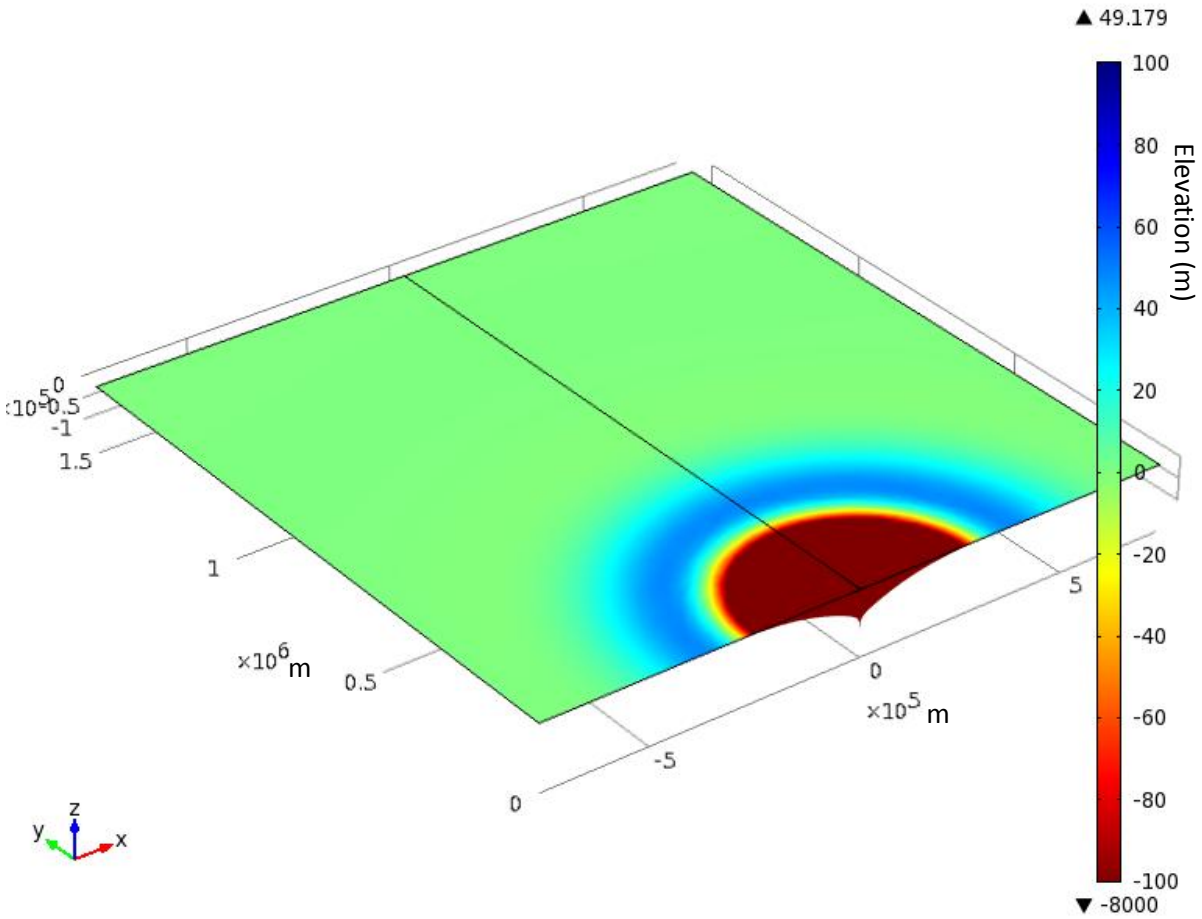

Figure 7 Numerical model of a point load with a given displacement.

3.3.3 Truncated Line Load

The model in Figure 8 represents a truncated line load. The truncated line begins at (0,0) m and ends at (0,500) m and is given a described displacement of 8000 m in the negative z direction, similar to the line load model in Figure 6. Once again this is appears as a dark red coloration in the model. The resulting bulge along the sides is very close in amplitude to that of the linear load, at 290 m in the positive z direction. However, the bulge around the point of truncation is significantly less than along the side. The coloration, of the model, indicates that the bulge, at the head (back left), is approximately 100 m in amplitude.

The boundary conditions of this model are described above. The displacement of the edges is the same as in Figure 7, with the edge at y = 0 m, parallel to the x axis, unbound to allow the deformation of flexure. Symmetry in Figure 8 is defined along the y = 0 m edge as well as a truncated edge that runs through the center of the plane.

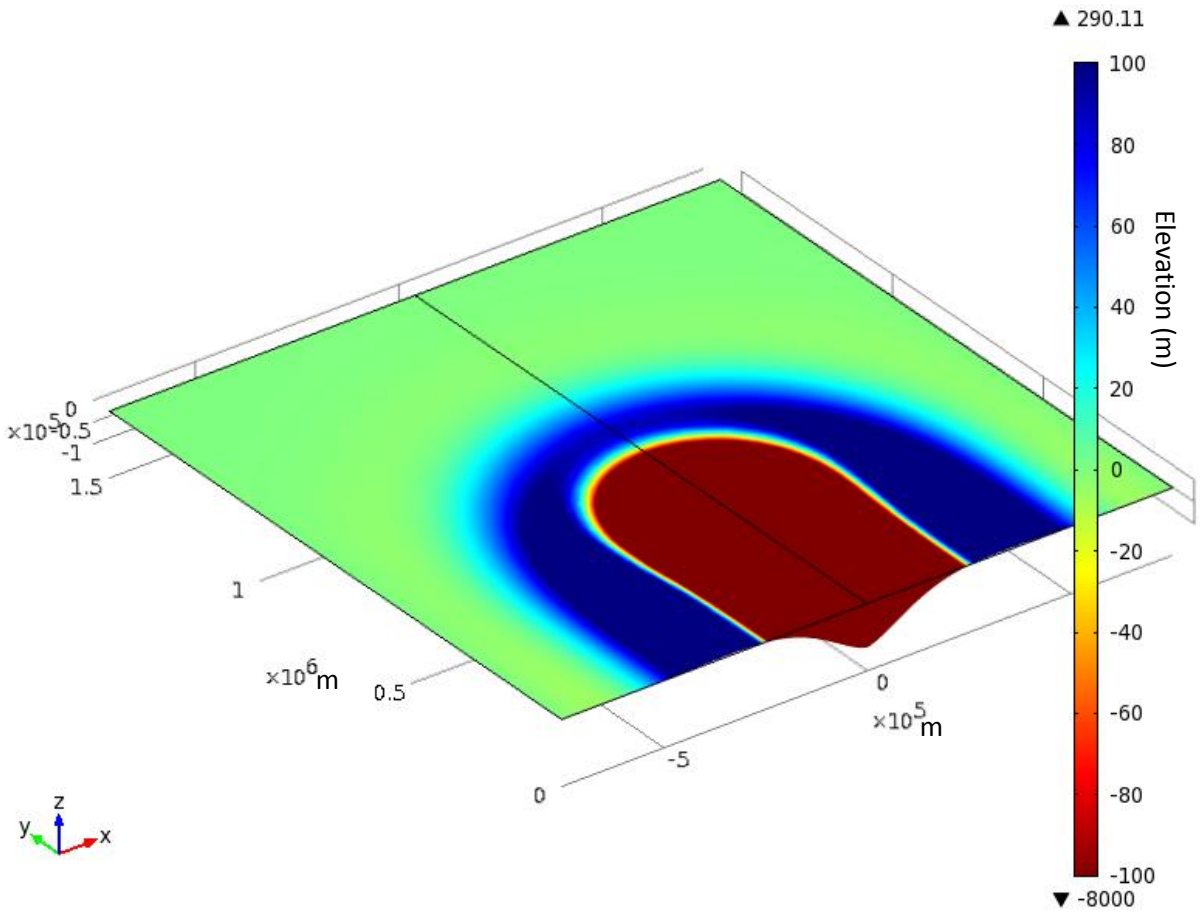

Figure 8 Numerical model of a truncated line load with a given displacement.

The truncated line model (Figure 8) resembles the occurrence around the Hawaiian Island swell. The bulge is ~290 m along the sides of truncated line while the coloration of the bulge around the point of truncation indicates the amplitude to be ~80 m. The amplitude of the bulge at the point of truncation is approximately 27% the amplitude compared to the side of the island chain.

Figure 9 is another model of the truncated line load. The boundary conditions of this model are the same as the model shown in Figure 8. However, the given displacement has been replaced with a line load. According to Watts (2001) the total volume of the Hawaiian island is 1.13×10^5 km^3. According to Watts (2001) the density of the volcanic deposit and the infill are both 2800 kg/m^3. This means that the mass of the head of the Hawaiian island chain is about 3.16×10^{11} kg. This value is used as the load displacement placed on the entire truncated line, under the influence of g defined in Table 1.

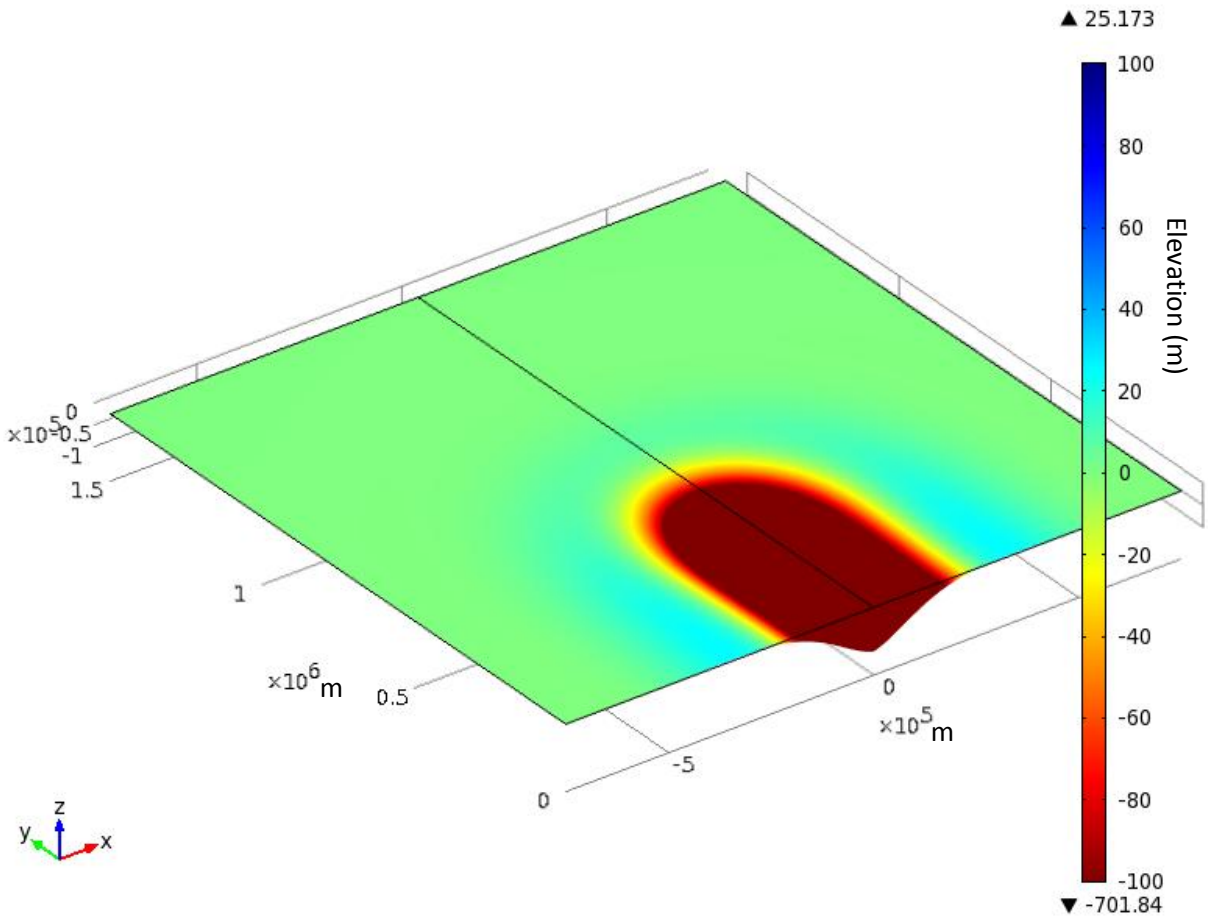

Figure 9 Numerical model of a truncated line load with an edge load.

Like the displacement model (Figure 8) and the bathymetric profiles (Figure 4a-c), the edge load model above (Figure 9) shows greater amplitude along the sides of the line load than along the point of truncation. The maximum amplitude along the sides is ~25 m while the amplitude around the point of truncation, according to the coloration, is ~5-10 m. This indicates the edge load model falls within the same 25-30% range of variation around the point of truncation.

4 Plumes

Mantle plumes are buoyant mantle upwelling believed to exist under volcanic centers. The basic shape of a rising plume is described as a long thin conduit connected to a large spherical head (Jellinek and Manga, 2004). Plume conduits remain connected to the hot boundary layer for longer periods of time compared to the time for an upwelling to ascend from a hot boundary through the full depth of an overlying fluid and feed more magma into the plume head. A typical mantle plume model is axisymmetric in nature with a large head and a narrow trailing conduit but very irregularly shaped (Figure 10) (Jellinek and Manga, 2004). However, in order for a plume to follow this model, there must be large variation of viscosity in the thermal boundary layer at the Core Mantle Boundary. The temperature of the plume is much greater than the surrounding mantle and above crust, because it forms and rises from the Core Mantle

Boundary. The heat of the plume transfers into the crust, causing it to become less dense (Sleep, 1992; Delaughter et. al. 2005; Davies, 1988). The variation in density allows for uplift to occur, giving further explanation to the cause of the swell.

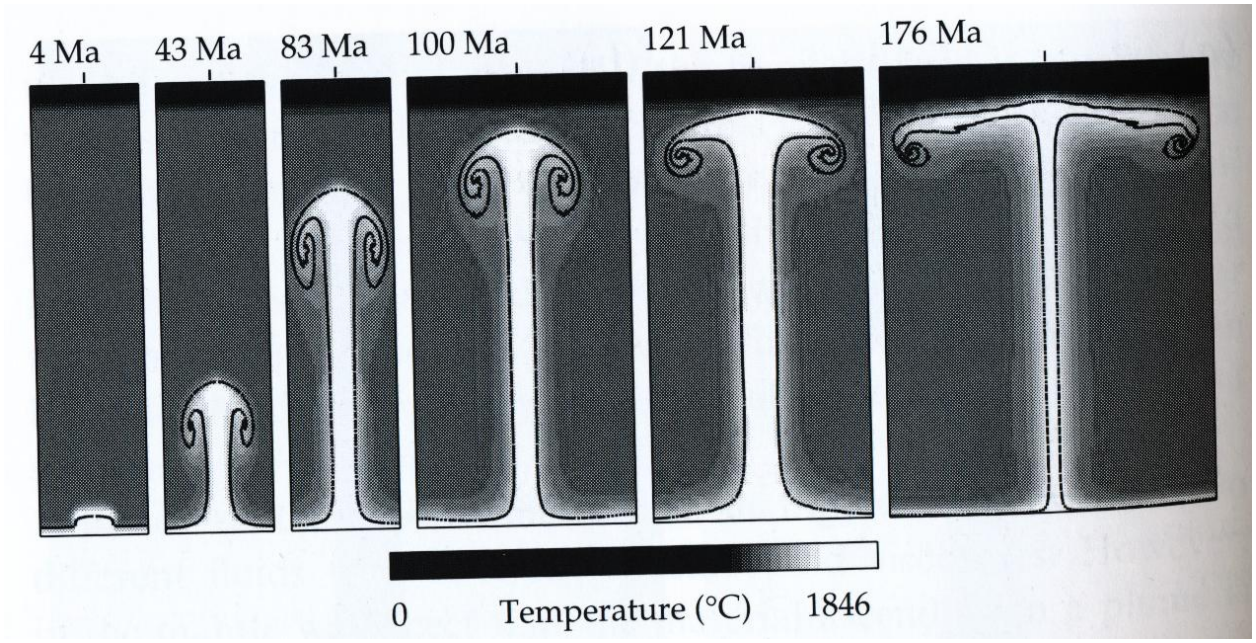

Figure 3 Numerical model of plume progression over 176 Ma (Davies, 1999).

According to Wilson (1963), the age of the islands increases traveling northwest along the chain. The change in age suggests that the islands form as the plate is pushed over a hotspot. The theory of plate tectonics assisting in the formation of the Emperor and Hawaiian Island chains is a widely accepted theory. The rate of tectonic plate separation compared to the amount and rate of deposition suggest an age of the Hawaiian Island chain of about 80 Ma (Cox, 1999; Watts, 2001; Zhong and Watts 2002).

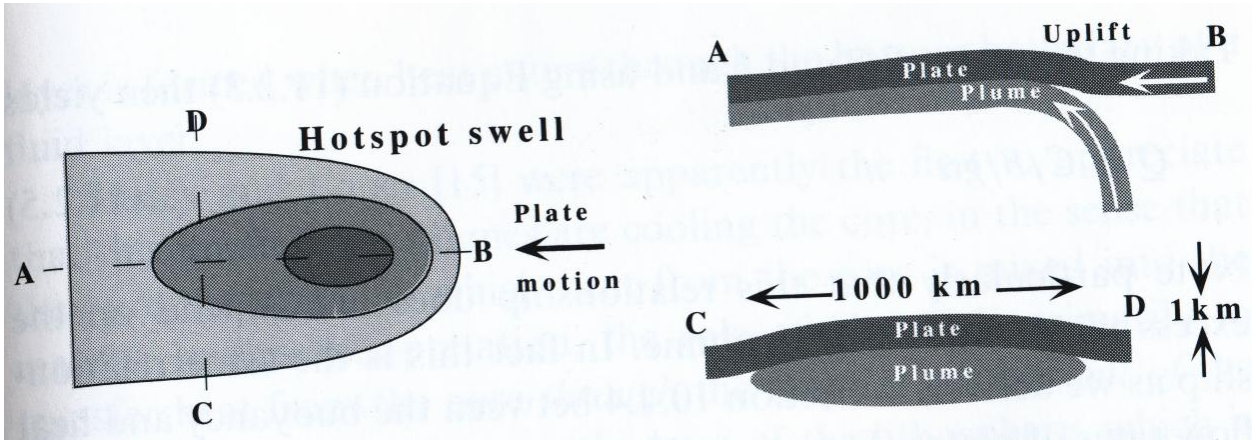

Figure 11 Representation of hotspot swell deflected by the motion of the plate (Davies, 1999).

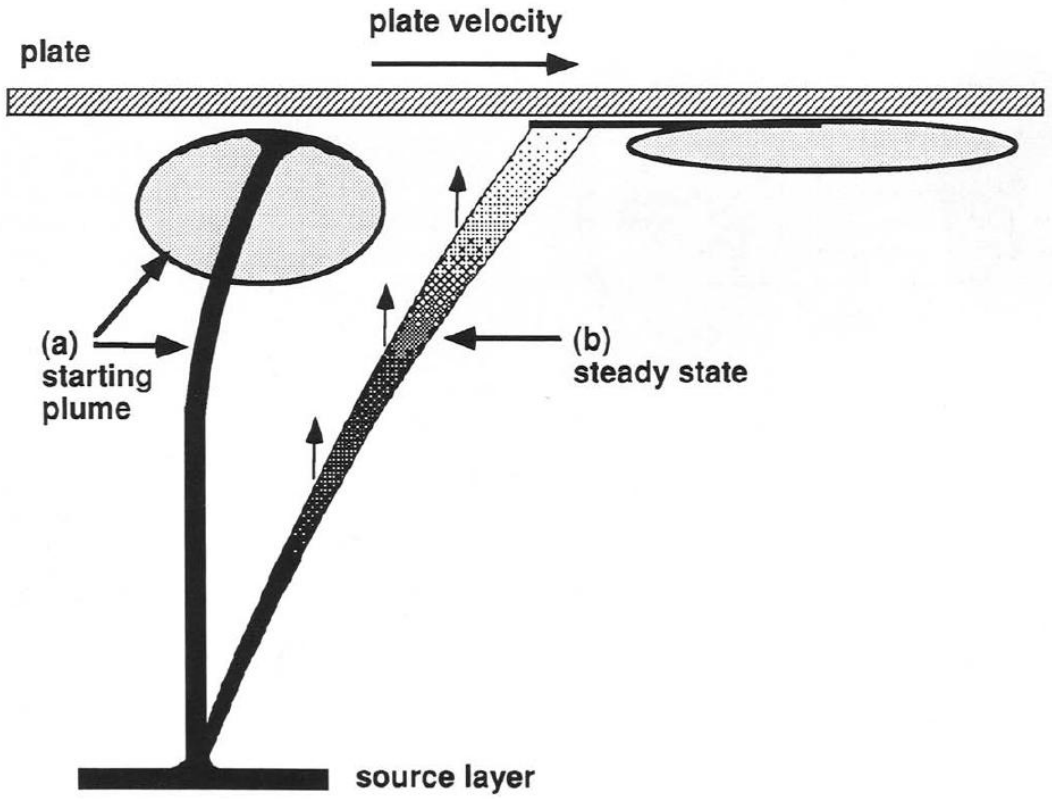

Figure 12 Representation of the plate motion deflecting the plume head and adjusting the steady state of the plume conduit (Griffiths and Campbell, 1991).

The plume head has now dissipated but a plume stem is still active underneath the islands. The dissipation of the plume head is most likely due to the influence of the tectonic plate above. The plume head is deflected by the tectonic plate to the northwest, as it moves atop the mantle represented by Figure 11 and Figure 12. If the amplitude of the Hawaiian swell is related to heating of the Pacific plate by the plume, it is possible that heating will be less important to the Southeast of the islands, as the plume is deviated away from there. Therefore, deflection of a mantle can provide an alternative explanation to the difference in swell amplitude to the Southeast and to the sides of the Hawaiian island chain.

Hypothesis 2: *The smaller amplitude of the Hawaii swell to the Southeast of the islands compared to the sides of the chain is due to deflection of the plume toward the northwest, following plate motion: heat delivery to the southeast of the chain is less than on the sides of the chain.*

4.1 Model setup

The physics necessary for the plume models include creeping flow and heat transfer.

Mantle flow is controlled by the Stokes equations:

Equation 8. $$\nabla \cdot V = 0$$

Equation 9. $$\nabla p + \eta \Delta v = \rho g$$

Equation 8 represents the incompressibility of the material and the second, Stokes equation (Equation 9), represents momentum balance in a fluid, neglecting inertia. The first term represents the gradient of dynamic pressure P. The second term in the Stokes equation is viscous stresses, where η is the viscosity and v the velocity of the fluid. Finally, the buoyancy of the fluid, given by the third term, with ρ the density of the fluid and g the acceleration of gravity.

In my models, the plume is driven by a temperature anomaly $\theta = T - T_r$, where T_r is the temperature of the ambient mantle. Removing a background lithostatic stress, I solve for a pressure and velocity variation p and v due to θ, which provide density anomalies $\rho_0 \alpha T$. Therefore, I solve for the following equations:

Equation 10. $$\nabla \cdot v = 0$$

Equation 11. $$\nabla p + \eta \Delta v = \rho_0 \alpha \theta g$$

The temperature anomaly obeys an advection/diffusion heat equation, given by,

Equation 12. $$\frac{\partial \theta}{\partial t} + v \cdot \nabla v = \kappa \Delta \theta$$

The three terms of this equation represent temperature change, advection and diffusion of heat, respectively, with κ the heat diffusivity given by $\kappa = k/\rho_0 C_p$, where *k* the heat conductivity and C_p is the heat capacity of the fluid. The value of these parameters is given in Table 1.

The model is structured as a 400 km by 500 km rectangle that acts as a window into the lithosphere. Symmetry is placed on the edge where x = 0 km for all y. This is because plumes are ideally symmetrical along their vertical axis. Open boundaries have been established along the bottom edge where y = -400 km and along the edge where x = 500 km. This simulates the constant source of flow from the core mantle boundary magma for the plume, beneath the bottom edge, as well as a direction for flow to easily go, at the right edge. The edge at the top of the model along y = 0 km is defined as a wall which flow cannot breach. This represents the underside of the Earth's crust, which the plume pushes up against, trying to breach the surface. Finally, a volume force is applied to the in the positive y direction over the entire work plane. The value of the force is defined as:

Equation 13. $$F = \rho_0 \alpha g T$$

where ρ_0 is density of the mantle, α is the coefficient of thermal expansion, g is gravity, and T is temperature defined by Equation 14.

The boundaries provided for heat transfer deal with temperature and flow direction. Symmetry lies along the same edge as it did in creeping flow. Outflow is defined along the right edge such that as the plume rises and reaches the surface, is does not continually accumulate beneath the top edge. The direction of the flow is represented by the blue arrows placed in Figure 9a-d. The size of the arrow indicates the magnitude of flow in the direction the arrow is pointing. The larger the arrow, the stronger the flow. The top and bottom edges are defined by set temperatures. The bottom edge is the provided heat source for the plume so it has a temperature of:

Equation 14. $$T = T_0 * e^{(-\frac{x}{w})^2}$$

Where T_0 is initial temperature and w is vertical displacement. The values of the variables for equations 13 and 14 are given in Table 1. This temperature boundary is opposed at the top edge by a temperature set at T = 0 K because the temperature on the underside of the Earth's crust is relatively much less than the temperature deep within the mantle.

The mesh overlaying this model is similar to the meshes used in the flexural models. Starting near the right and top edges, the triangular mesh is extremely fine, providing a larger number of data points to collect information. Once again, a coarser mesh, meaning fewer data points, is more acceptable the further away from the edge the data point is.

The 2D plume model is also time dependent . Starting at time t = 0 s, the model progresses to a final time t = 20 Myr. Shown in Figures 9a-d below are various stages of the plume starting at t = 0 s (Figure 12a) and progressing to time t >> 0 s (Figure 12b).

4.1.1 2D Plume Model

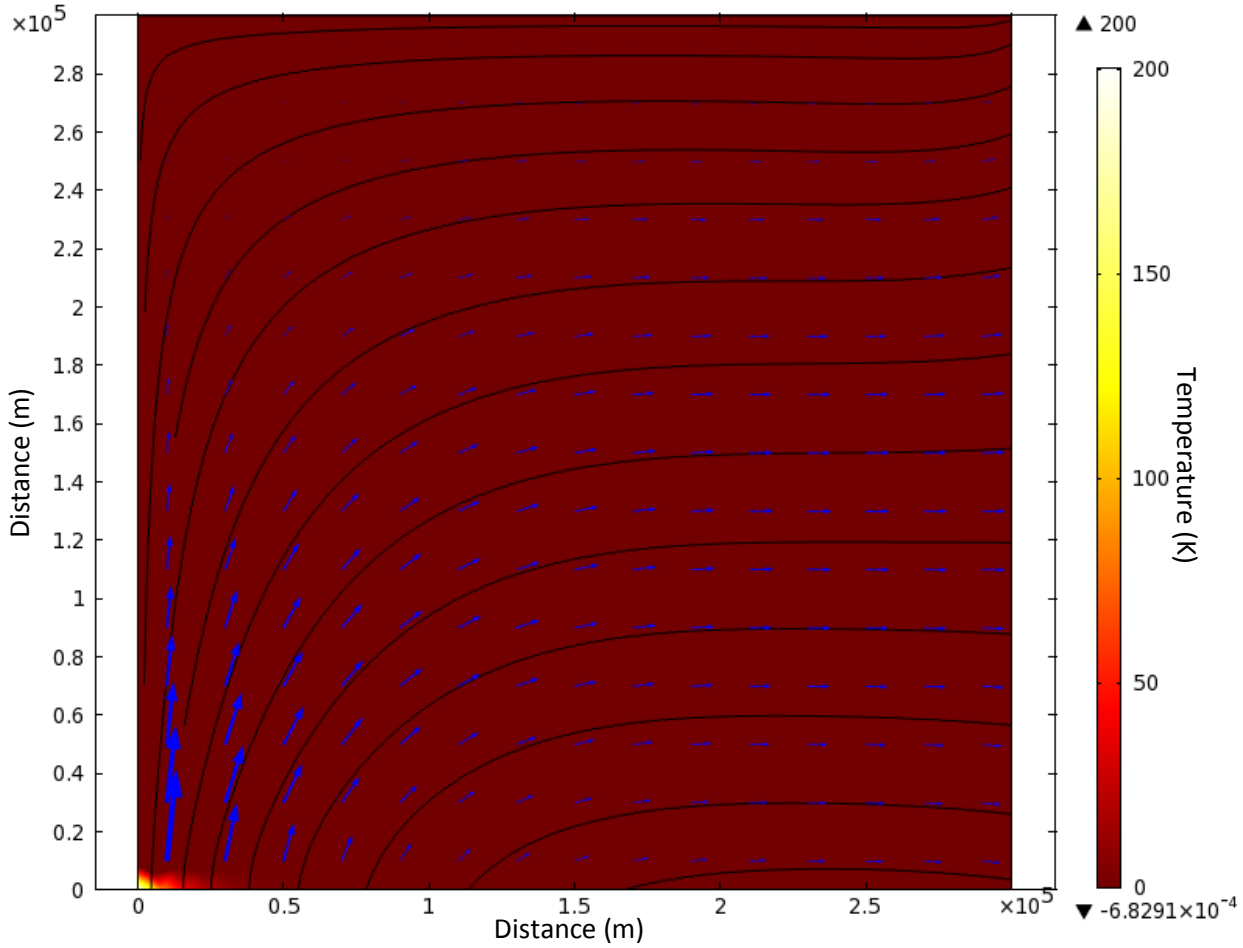

Figure 13a. 2D plume model at time t = 0 Myr.

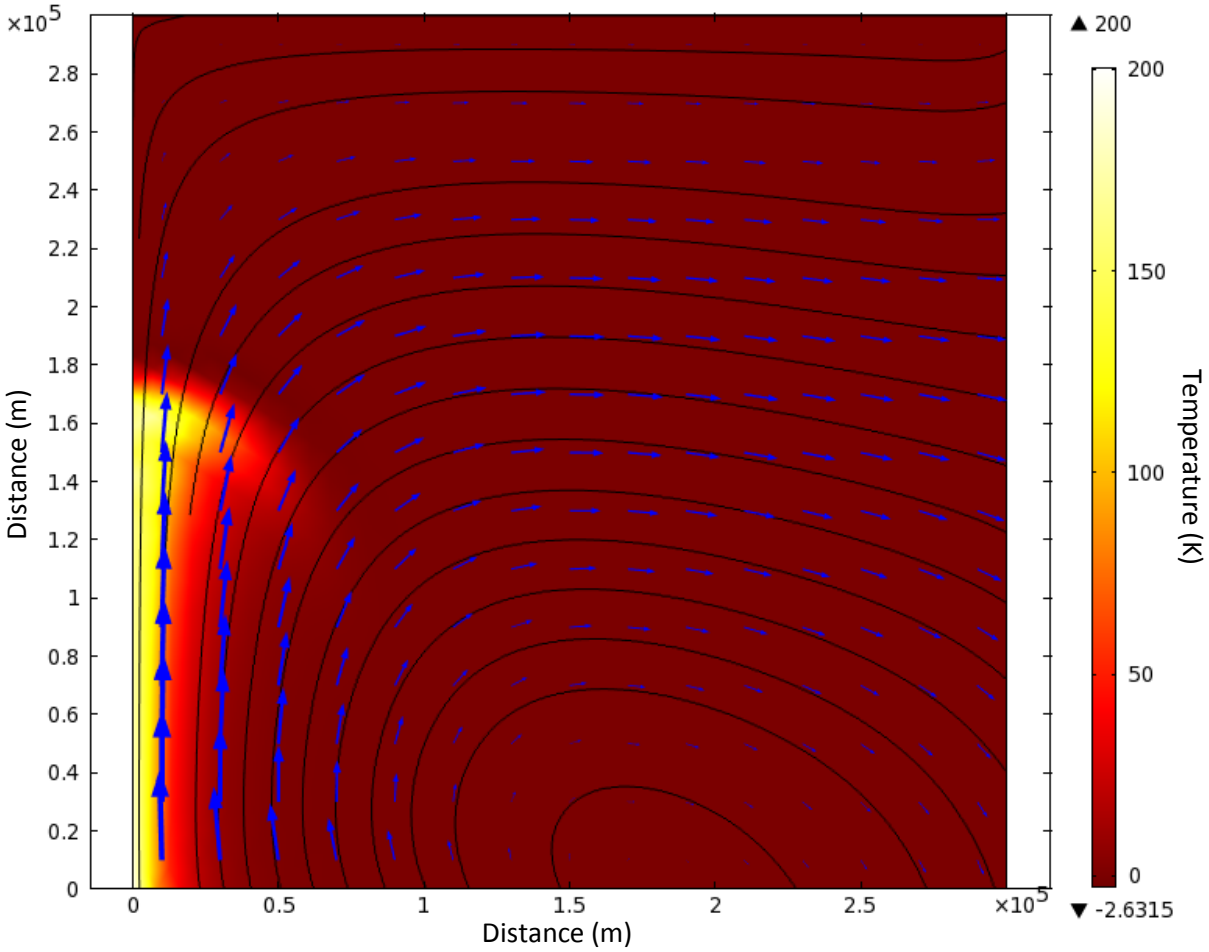

Figure 13b. 2D plume model at time t >0.

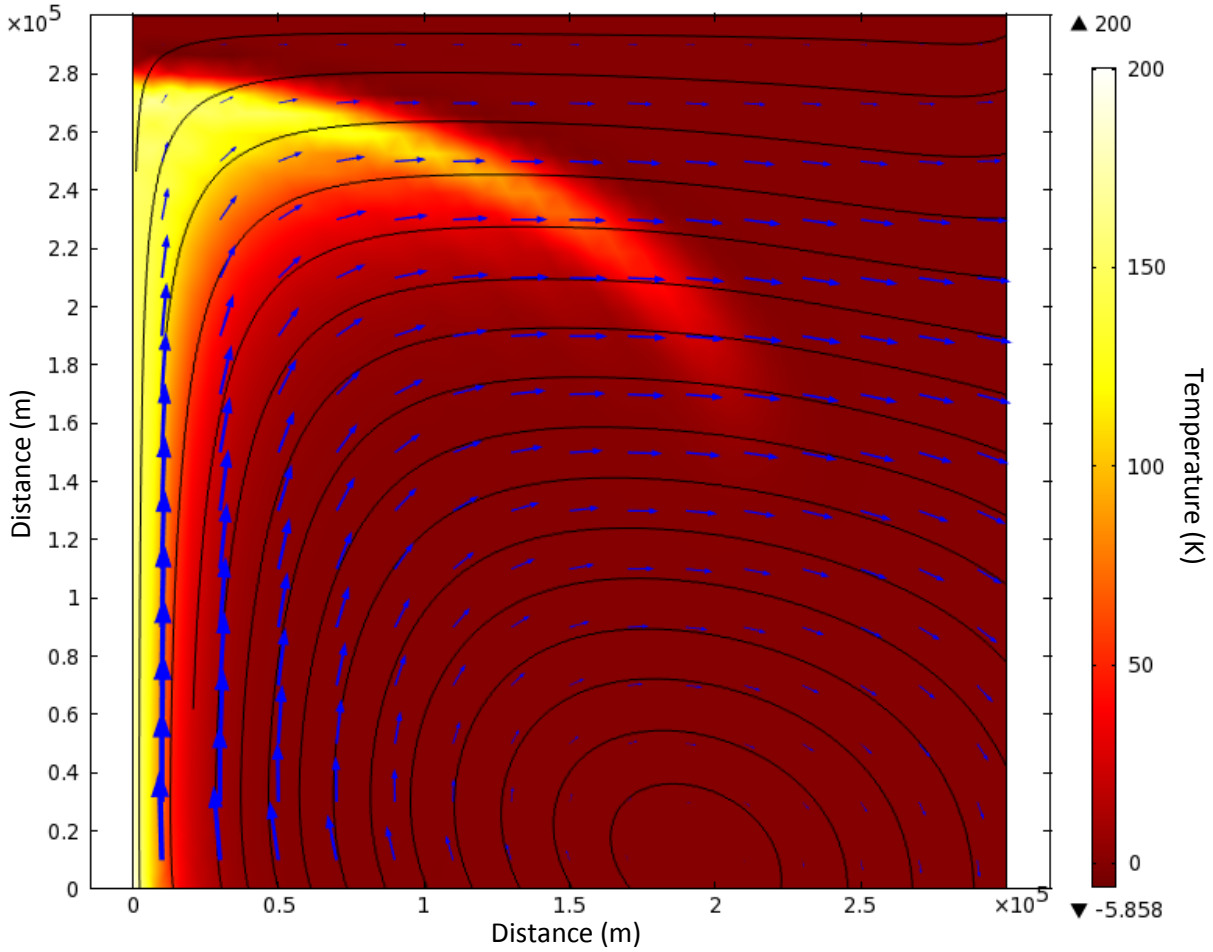

Figure 13c. 2D plume model at time t>>0.

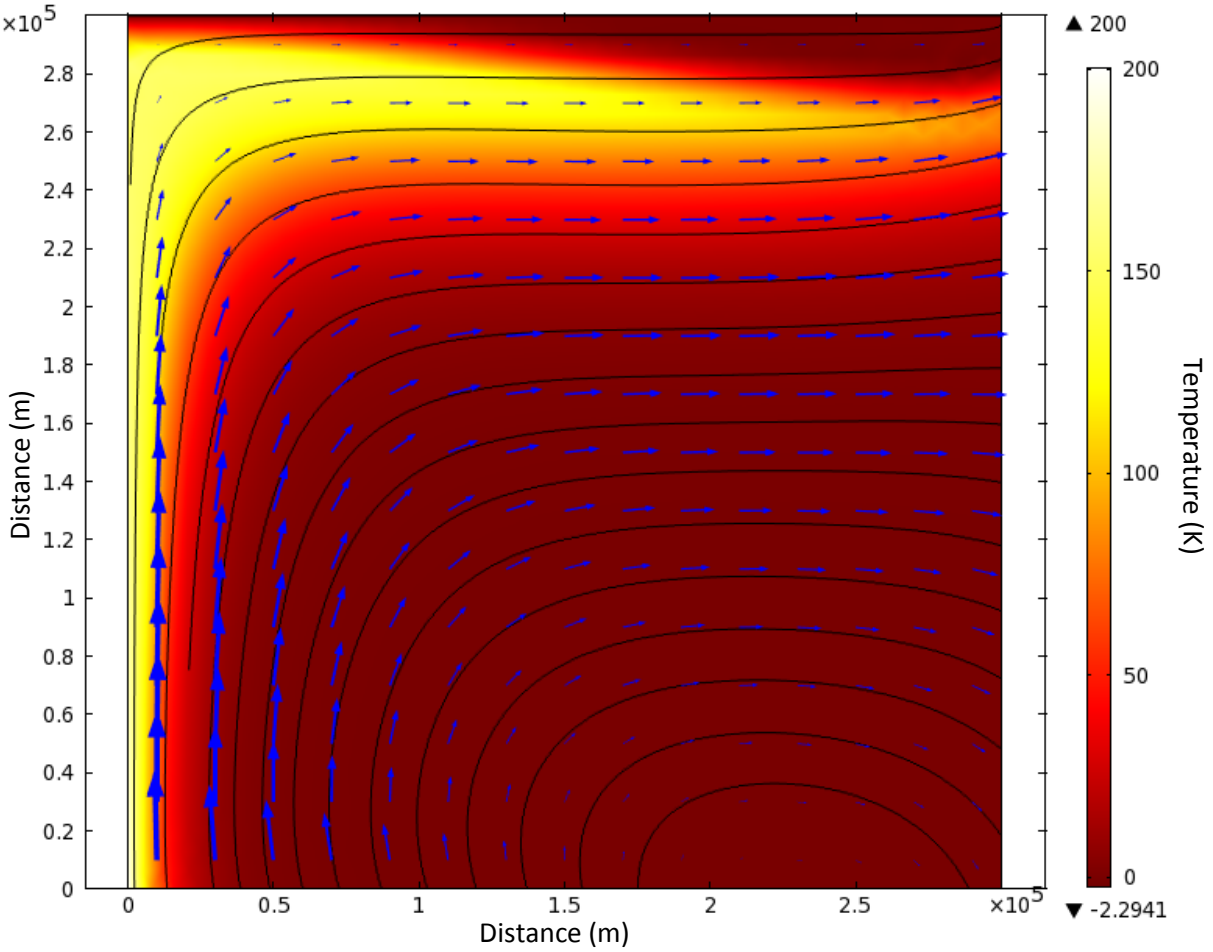

Figure 13d. 2D plume model at time t=15Myr

Figure 12a-d model the progression of the plume over 15 Myr. As seen in the figures, as the plume rises, it obtains a spherical head followed by a thin conduit (Figure 13b). The conduit is still connected to the initial heat source, which continually feeds the plume as it rises. As the plume hits the underside of the crust, the heat begins to spread. The blue arrows indicate direction of heat flow, which, when close to the heat source, is parallel to the y-axis. As distance from the conduit increases, the direction of flow changes, becoming more perpendicular to the y axis as x increases.

The plume imposes a normal stress on the underside of the plate, which must be balanced by a topographic load. Figure 14 shows dynamic topography, the topography that would be necessary to balance this load, ignoring elastic flexure, and assuming a density difference between crust and ocean of 2000 kg/m^3. A flexural bulge would be superposed on top of this dynamic topography. Therefore, if dynamic topography is different along the sides of the Hawaiian island chain compared to the end of the chain, this would also generate variations in swell amplitude similar to the observations.

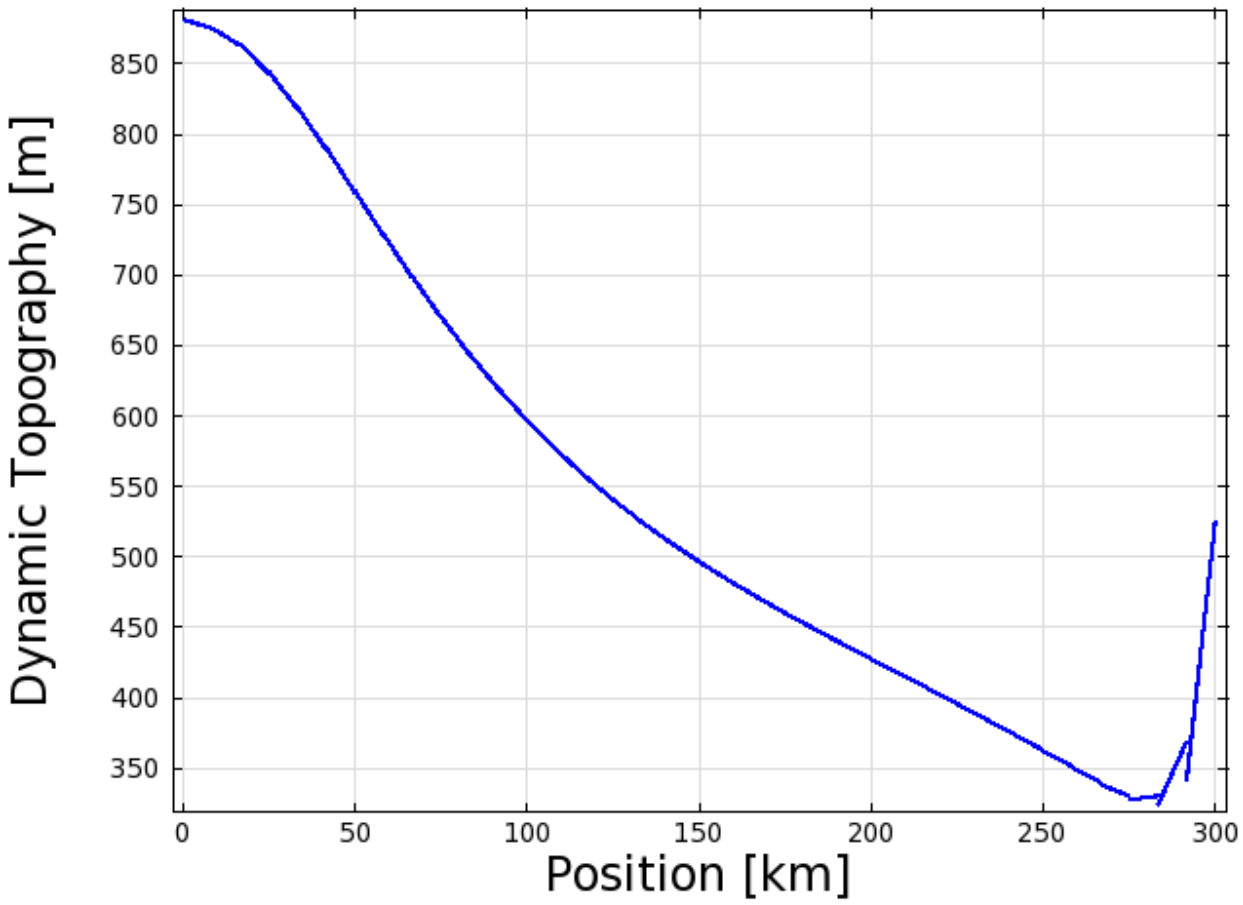

Figure 14. Profile showing the deflection of the lithosphere under the influence of normal stresses induced by the plume on the underside of the plate.

4.1.2 3D Plume Model

The 3D plume model flows the same physics as the 2D model. The boundary conditions were expanded to confine the plume to a 3D prism (Figure 15). The dimensions of the prism are $x = 1 \times 10^6$ m, $y = 2 \times 10^6$ m, and $z = 1 \times 10^6$ m and the plume begins at a point placed on x = 0 m, y = 0 m and z = 0 m. The amount of time the plume is progressing was increased to 100Myr to insure that the plume could fully progress. The mesh placed on this model is normal. The light blue lines show the flow direction of heat.

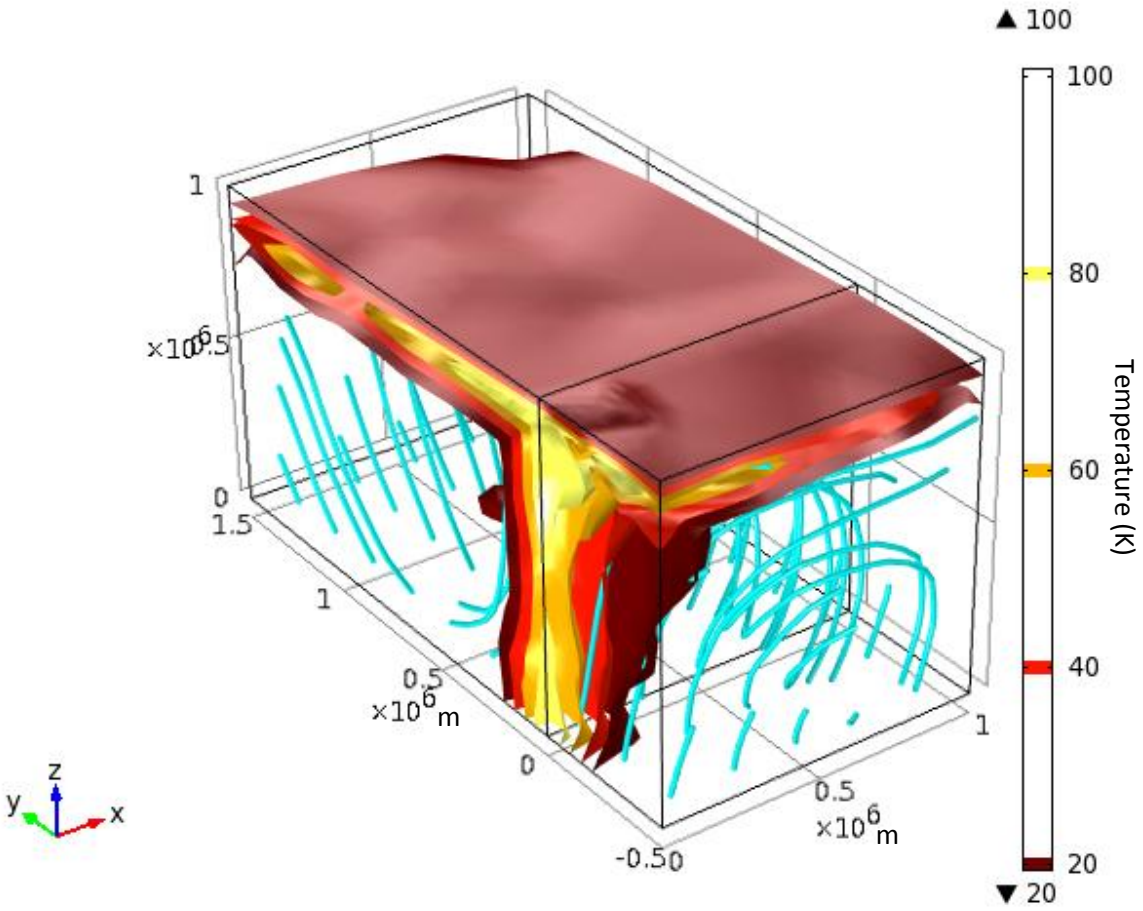

Figure 15. Plume model showing the progression of the plume over 100 Myr in 3 dimensions.

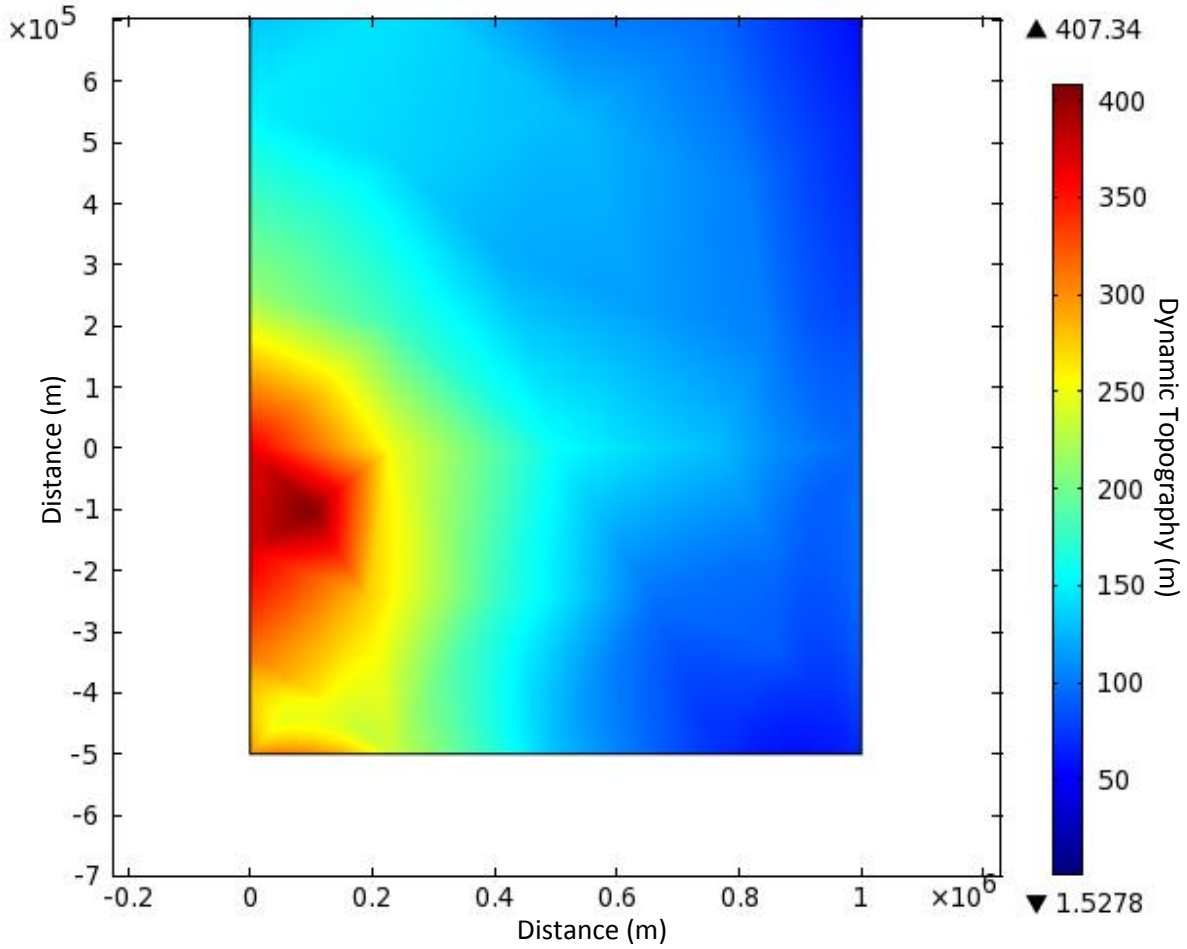

Figure 16 Topographical view showing the deflection of the lithosphere under the influence of normal stresses induced by the plume on the underside of the plate in the 3D model.

This is a topographical view of the dynamic topography caused by the plume. As seen the plume pushes up on the underside of the plate and cause a swell of ~400 m indicated by the red occurring at (0.1,-1). The movement of the plume conduit and head in the model can be explain by the boundary conditions. There is greater pressure created by the heat flow of the plume in the positive y quadrant. This pressure pushes the conduit and the head of the plume in the negative y direction giving one possible explanation to the offset of the plume head. The indication of swell seen at (-5,0) is a numerical anomaly. It is uncertain what is causing this anomaly to happen but if the plume box were to be expanded in the negative y direction it would most likely dissipate . The next step was add slip, at a given rate, to deflect the plume.

4.1.3 3D Plume Model with Plate Motion

The model in Figure 17 has identical boundary condition as the model in Figure 15 above. In addition the top wall which previously had no slip now has a slip of 13 cm/yr similar to Moore et al.,1998. This represents the motion and rate of the seafloor spreading. The results are shown in Figure 17 and 18.

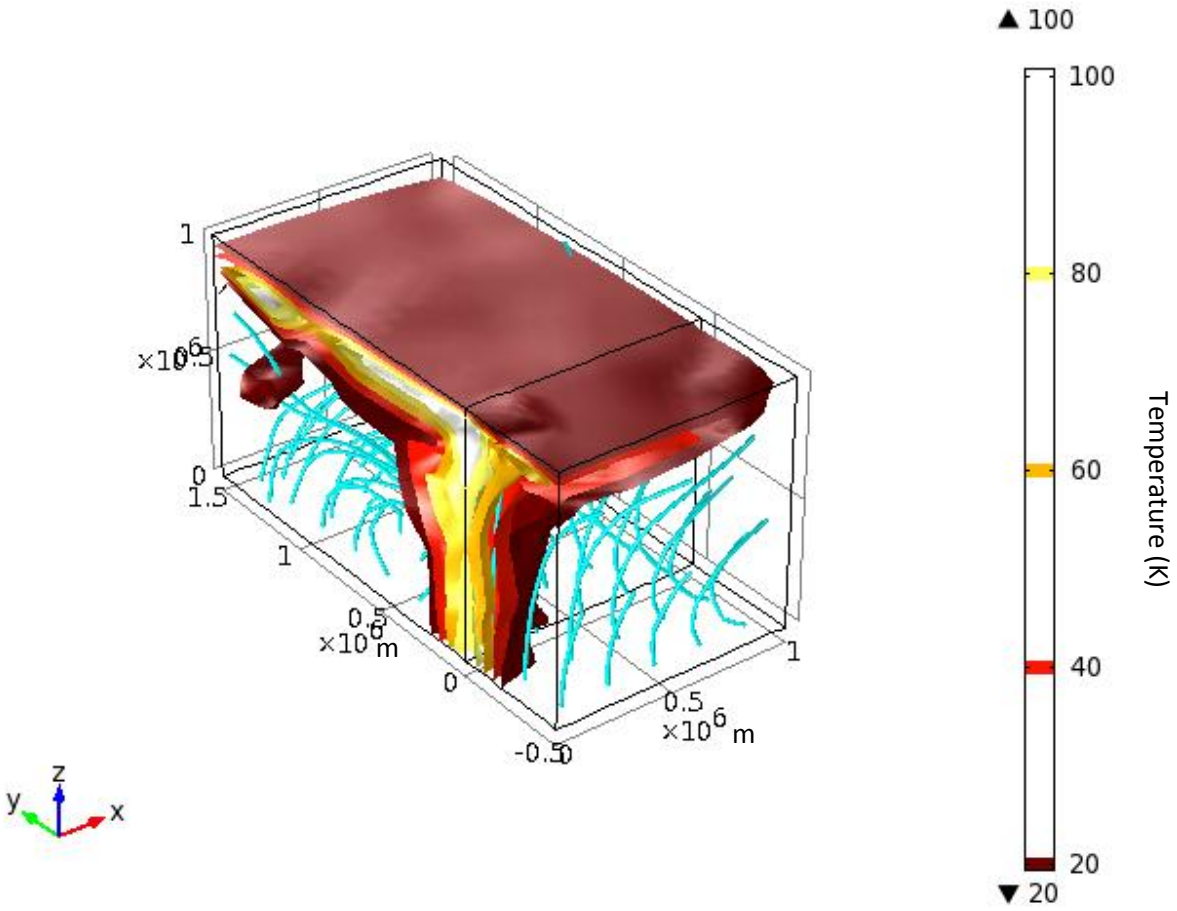

Figure 17. 3D plume model with added plate motion at the top of 13 cm/yr

Deflection of the plume can be seen given the location of the swell in Figure 17. Unlike the swell in Figure 16 the swell in Figure 18 is closer to laying on the coordinates (0,0). However, in Figure 17, the light blue lines still indicated heat flow bending the conduit of the plume in the negative y direction. This indicates that the plate motion in the positive y direction is deflecting the head of the plume but only slightly.

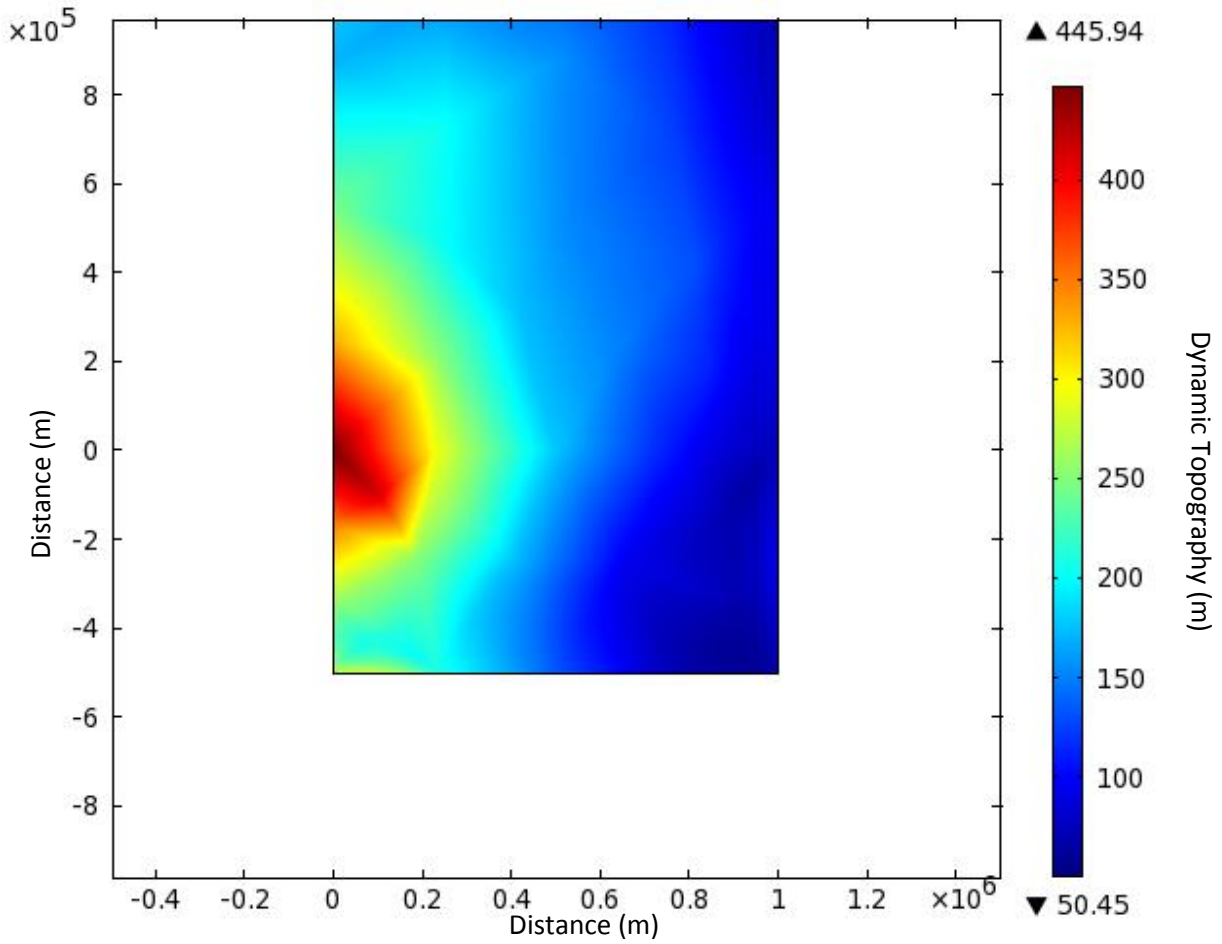

Figure 18. Topographical view showing the deflection of the lithosphere under the influence of normal stresses induced by the plume on the underside of the plate in the 3D model. The plume is being slightly deflected in the positive y direction by added motion.

The minimal deflection of the plume can possibly be explained by the velocity of the plume compared to the velocity of the plate motion. The model indicated the plume was moving ~60 cm/yr by the time it has reached the underside of the plate. This is much greater than the motion of the plate. Therefore I increased the motion of the plate to 130 cm/yr. Though this is unrealistic, in the sense of the plate motion, the results, seen in Figure 19, shows the deflection of the plume.

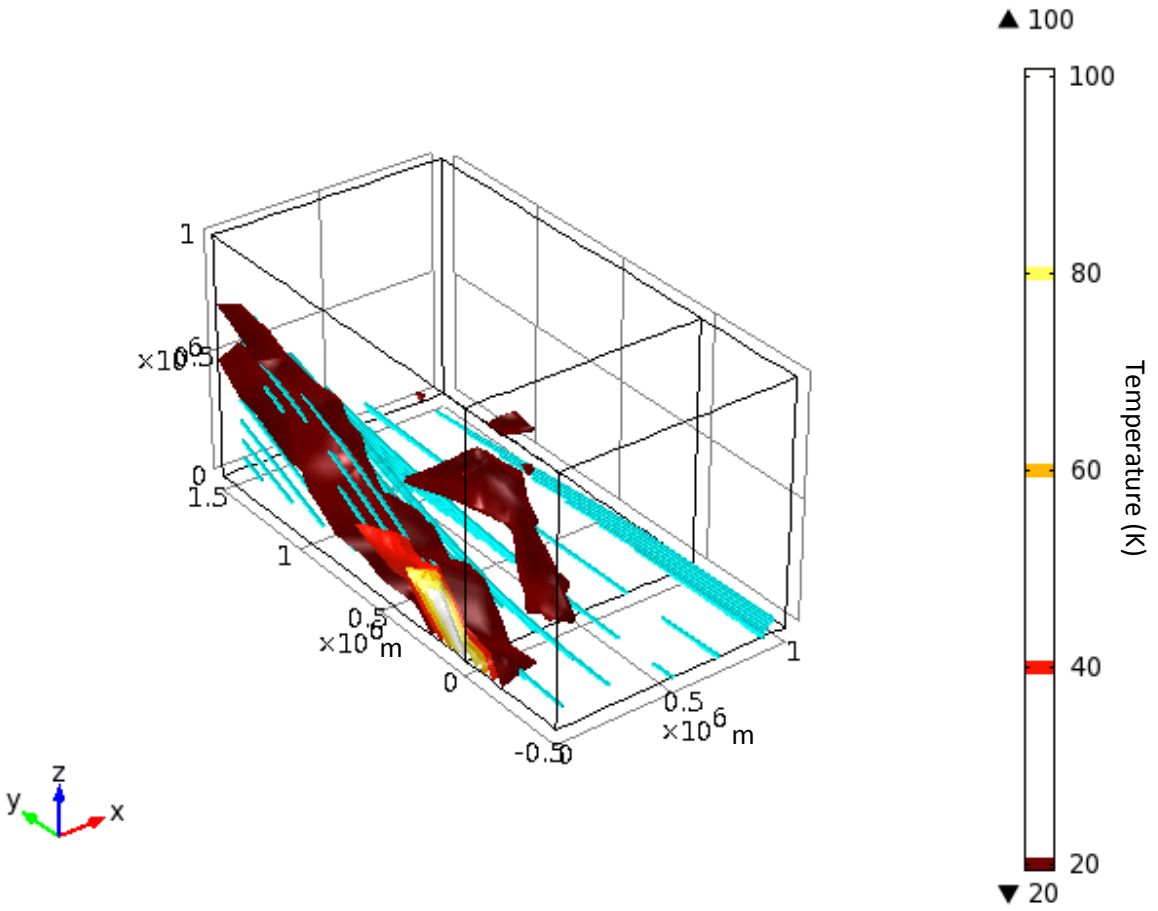

Figure19. 3D plume model showing the deflection of the plume by the motion of the plate in the positive y direction.

Analysis of the dynamic topography in Figure 20 shows that the amplitude of swell is greater in the y direction than at the point the plume rises. However, the variation in this amplitude does not appear to be similar to that of the Hawaiian swell. Therefore, these 3D plume models, do not support the hypothesis of swell variation due plume deflection and heat transfer.

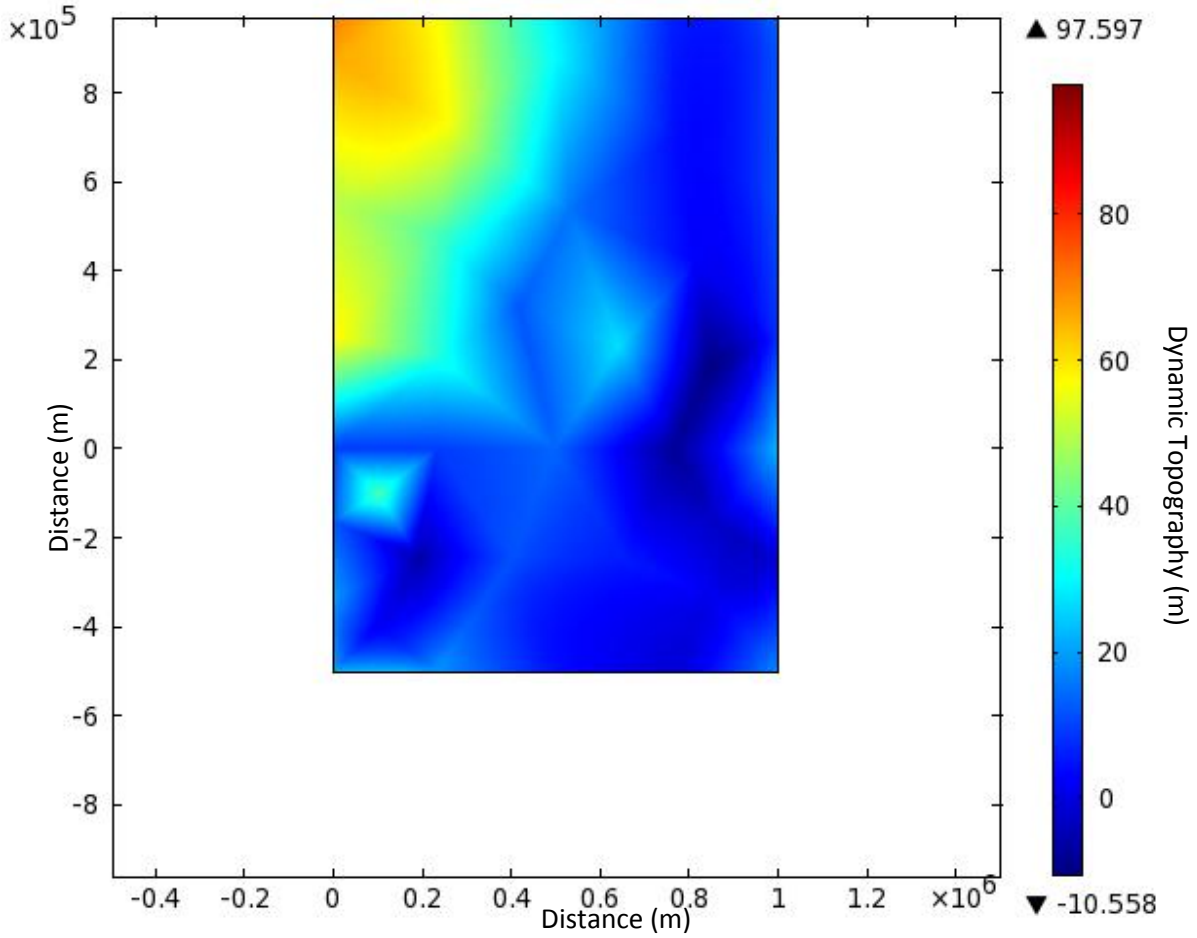

Figure 20. Topographical view showing the deflection of the lithosphere under the influence of normal stresses induced by the plume on the underside of the plate in the 3D model. The plume is being slightly deflected in the positive y direction by added motion.

5 Conclusion

I propose that the origin of the swell, around the Hawaiian Islands, is produced by flexure due to the load of the Hawaiian Island chain. Another hypothesis for the origin of the amplitude swell is given by heat transfer from the hot spot below, which is greater along the sides, than the southeast of the island chain. Bathymetric profiles show that the swell at the head of the Hawaiian Island chain is ~30% the amplitude of the swell along the side. Flexural models support the variation in swell amplitude. The truncated line models showed greater bulge amplitude along the side of the displacement. The bulge around the point of truncation, in both the set displacement and the line load model, were within the 25-30% range. My modeling is consistent with the hypothesis that flexure has an effect on the variation in amplitude around the Hawaiian swell.

The 3D plume models show that through heat transfer greater swell amplitude is obtained. However, by adding plate motion to deflect the plume the variation seen in swell amplitude is dissimilar to the swell of the Hawaiian island. The variation of the swell seen is

~50-60% which is not consistent with the 25-30% seen around the Hawaiian island chain. Therefore, my modeling is not consistent with my hypothesis that deflection of the plume head by plate motion is the prominent cause of the variation in swell amplitude.

6 References

(additional references to be added)

Abramowitz, M. and Stegun, I. A. (Eds.), Handbook of Mathematical Functions with Formulas, Graphs, and Mathematical Tables, 9th printing. New York: Dover, 1972

Asaadi, N., and N. Ribe, and F. Sobouti. "Inferring nonlinear mantle rheology from the shape of the Hawaiian swell." Nature 473 (2011): 501-506.

Banerdt, Bruce W., Matthew P. Golombek, Kenneth L. Tanaka. "Stress and Tectonics on Mars". Mars (1992): 249-297.

Brotchie, J. F., and Silvester, R., 1969, On crustal flexure: J. Geophys. Res, v. 74, pp. 5240-5245.

Cox, R. T. "Hawaiian volcanic propagation and Hawaiian swell asymmetry: evidence of northwestard flow of deep upper mantle." Tectonophysics 310, 1999: 69-79.

Davies, Geoffrey F. "Ocean Bathymetry and Mantle Convection 1. Large-Scale Flow and Hotspots." Journal of Geophysical Research 93 (1988): 10467-10480.

Davies, Geoffrey F. Dynamic Earth Plates Plumes and Mantle Convection. Cambridge: Cambridge University Press, 1999.

DeLaughter, John E., and Carol Stein, and Seth Stein. "Hot Spots: A view from the swells." Geological Society of America (2005): 257-278.

Griffiths, Ross W, and Mark Richards. "The Adjustment of mantle Plumes to Changes in Plate Motion." Geophysical Research Letters 16 (1989): 437-440.

Jellinek, A M, and Michael Manga. "Links Between Long-Lived Hot Spots Mantle Plumes, D", and Plate Tectonics." American Geophysical Union, 42, 2004.

"Kelvin Function of the Second Kind." Keisan. 2012. 16 Mar. 2012. <http://keisan.casio.com/has10/SpecExec.cgi?id=system/2006/1222673844>.

Lliboutry, Louis. Quantitative Geophysics and Geology. Editeur, Paris: Masson, 1999.

Mitchell, G., Montési, L., Zhu, W., Smith D.K. and H. Schouten Transient rifting north of the Galápagos Triple Junction, Earth Planetary Science Letters, 2011.

Moore, William B, and Gerald Schubert, and Paul Tackley. "Three-Dimensional Simulations of Plume-Lithosphere Interaction at the Hawaiian Swell." Science 279 (1998): 1008-1011.

Montési, L.G.J., M.D. Behn, L.B. Hebet, J. Lin, J. Barry, Controls on melt migration and extraction at the ultraslow Southwest Indian Ridge 10°-16°E, Journal of Geophysical Research, 116, B10102, 2011.

Sleep, Norman H.. "Hotspot Volcanism and Mantle Plumes." Annu. Rev. Earth Planet. Science 20 (1992): 19-23.

Sleep, Norman H.. "Hotspots and Mantle Plumes: Some Phenomenology." Journal of Geophysical Research 95 (1990): 6715-6736.

Stacey, F. D., and P. Davis. Physics of the Earth. Cambridge, MA: Cambridge University Press, 2008.

Turcotte, Donald L., and Gerald Schubert. Geodynamics. Cambridge, MA: Cambridge University Press, 2002.

Watts, A. B. Isostacy and Flexure of the Lithosphere. Cambridge, MA: Cambridge University Press, 2001.

Wessel, Pal. "A Reexamination of the Flexural deformation Beneath the Hawaiian Islands." Journal of Geophysical Research 98 (1993): 12,177-12,190.

Whitehead, John A., and Douglas Luther. "Dynamics of Laboratory Diapir and Plume Models." Journal of Geophysical Research 80 (1975): 705-717.

Wilson, J. Tuzo. "A possible Origin of the Hawaiian Islands." Canadian Journal of Physics, 1963, 41(6): 863-870, 10.1139/p63-094.

Wilson, J. Tuzo "Mantle Plumes and Plate Motion." Tectonophysics 19 (1973): 149-164.

Wilson, M. Igneous Petrogenesis a Global Tectonic Approach. London: Academic Division of Unwin Hyman Ltd, 1989.

Zhong, Shijie, A. B. Watts. "Constraints on the dynamics of mantle plume from uplift of the Hawaiian Islands." Earth and Planetary Science Letters, 203, 2002: 105-116.

7 Acknowledgements

I'd like to thank Dr. Laurent Montesi for his guidance through the writing of this proposal. His devotion of time and knowledge help greatly throughout my efforts of GEOL393. I would also like to thank the Professors in the Department of Geology for their comments based on my February presentation. Finally, I would like to thank Natalie Sievers, Chris Salata, and Dr. Phil Candela for their peer review of my proposal.

.

8 Appendices

8.1 Appendix A

Topographic and bathymetric profiles around the Hawaiian Island chain excluding those provided in Figures 3a-c. Figure 3a is the topographic profile between Figure 10b and Figure 10c. Figure 3b is the topographic profile between Figure 10d and Figure 10e. Figure 3c is the topographic profile taken farther northwest than Figure 10g. Each topographic profile is followed by its corresponding bathymetric profile, of the cut taken, in Appendix B.

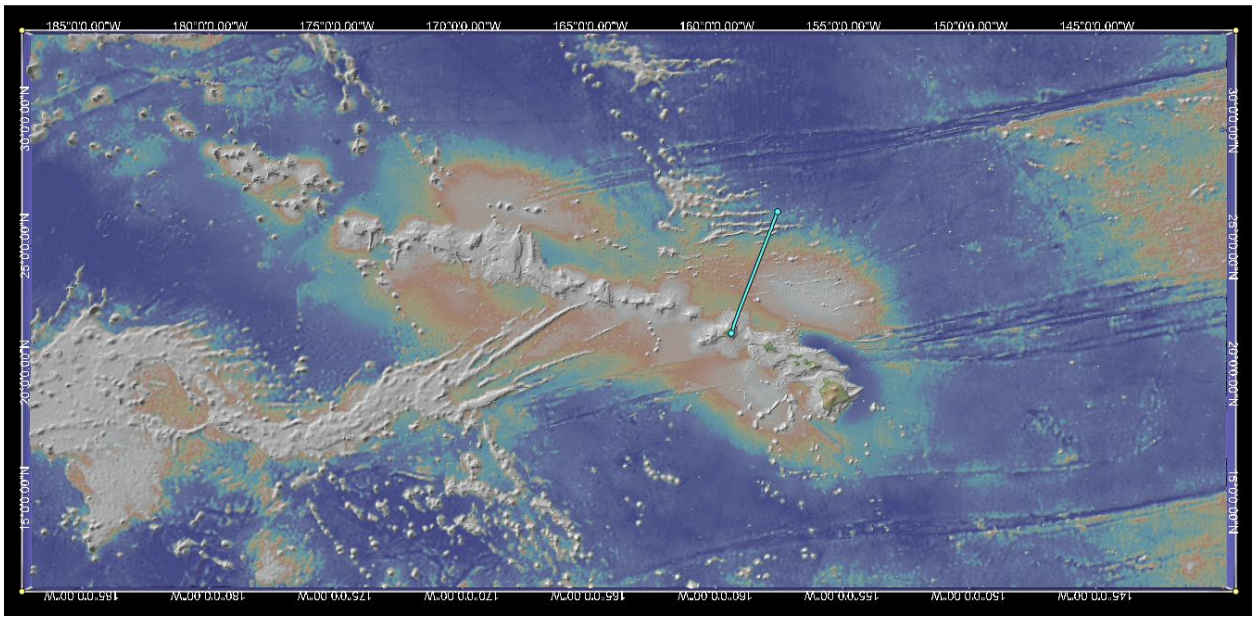

Figure 21a.

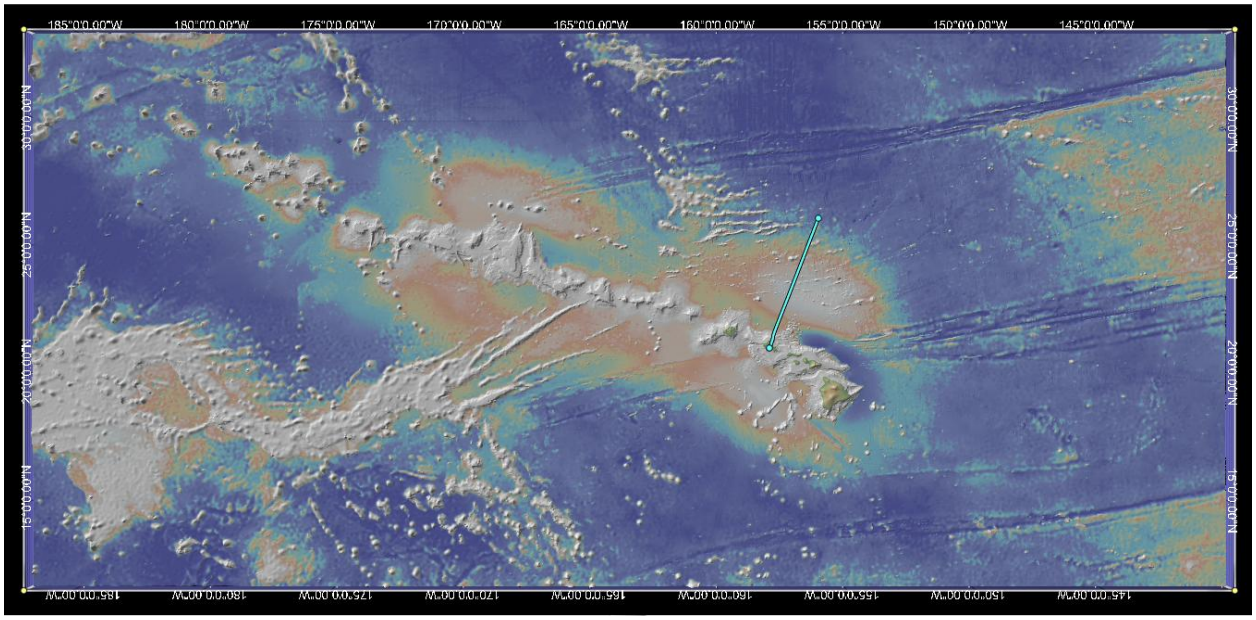

Figure 21b.

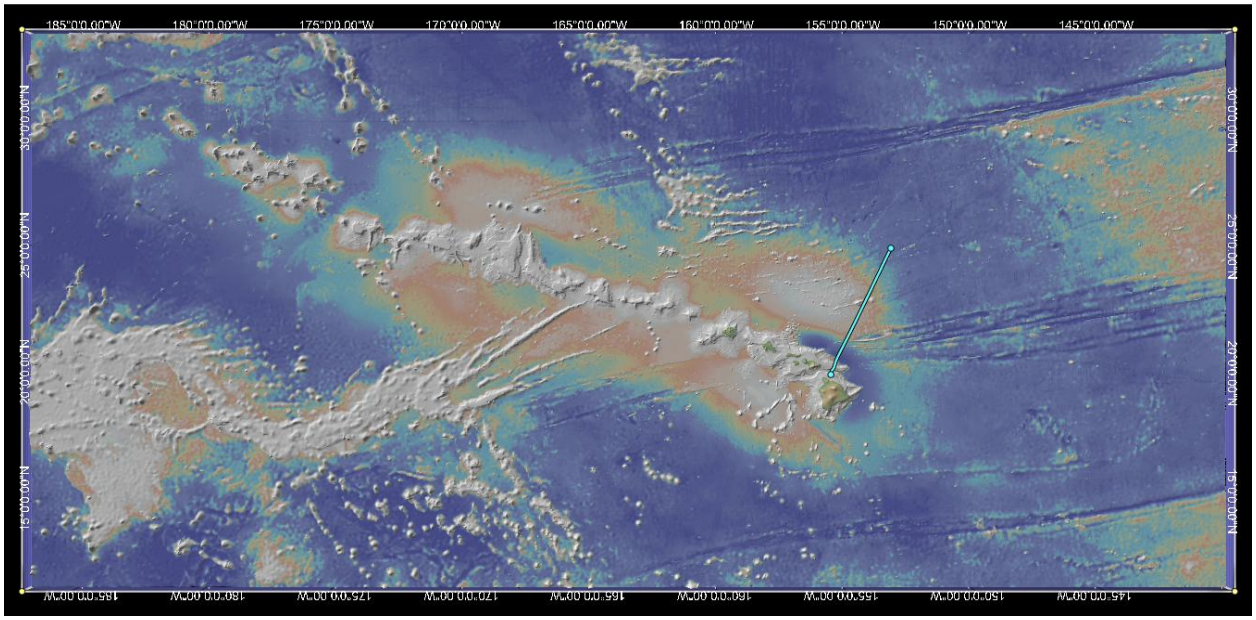

Figure 21c.

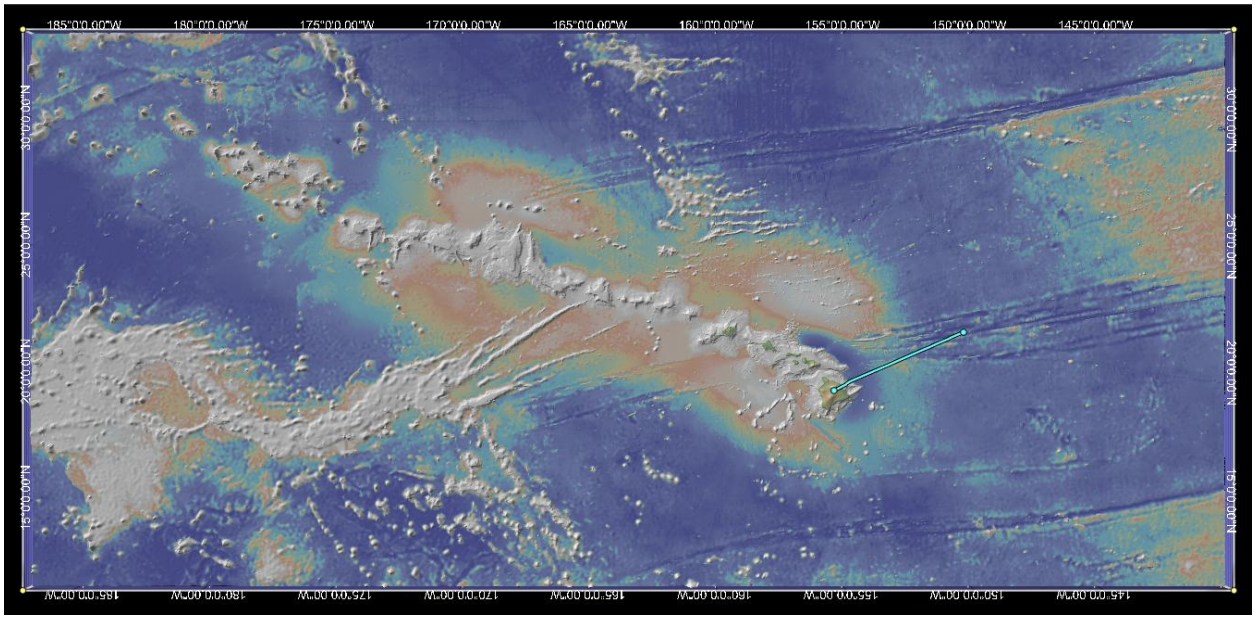

Figure 21d.

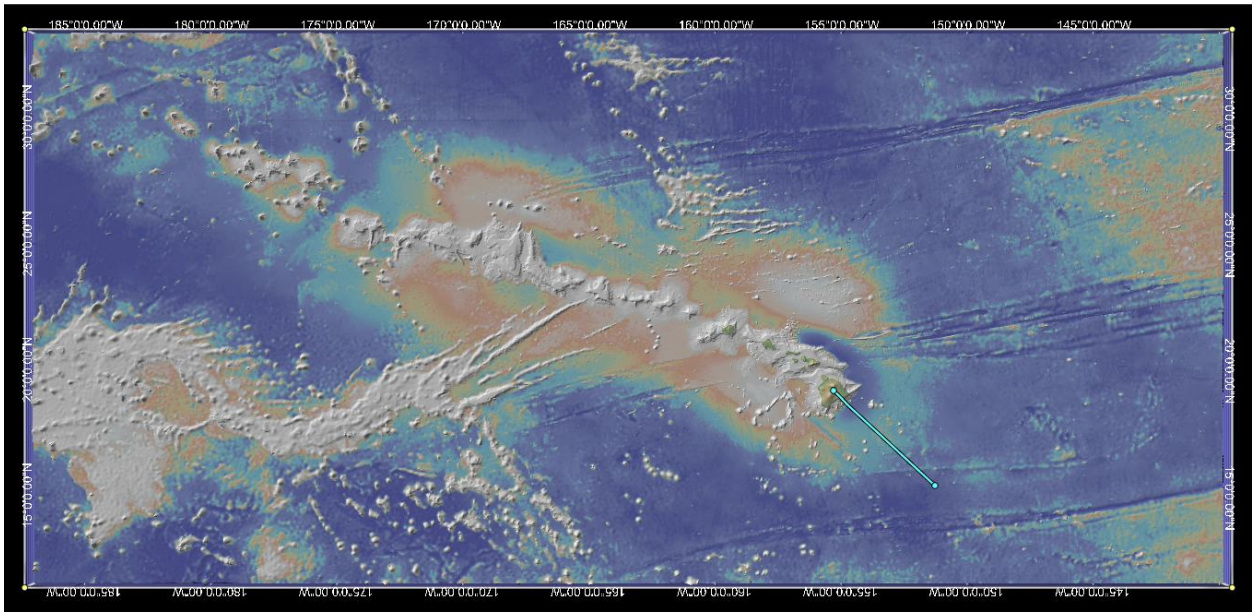

Figure 21e.

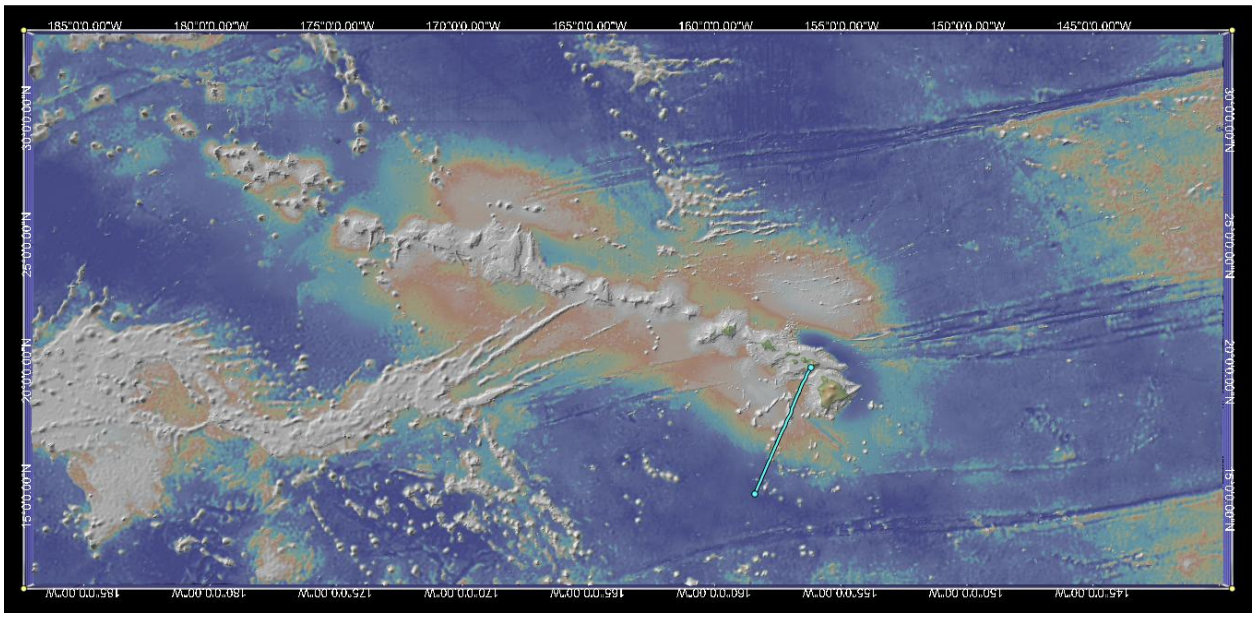

Figure 21f.

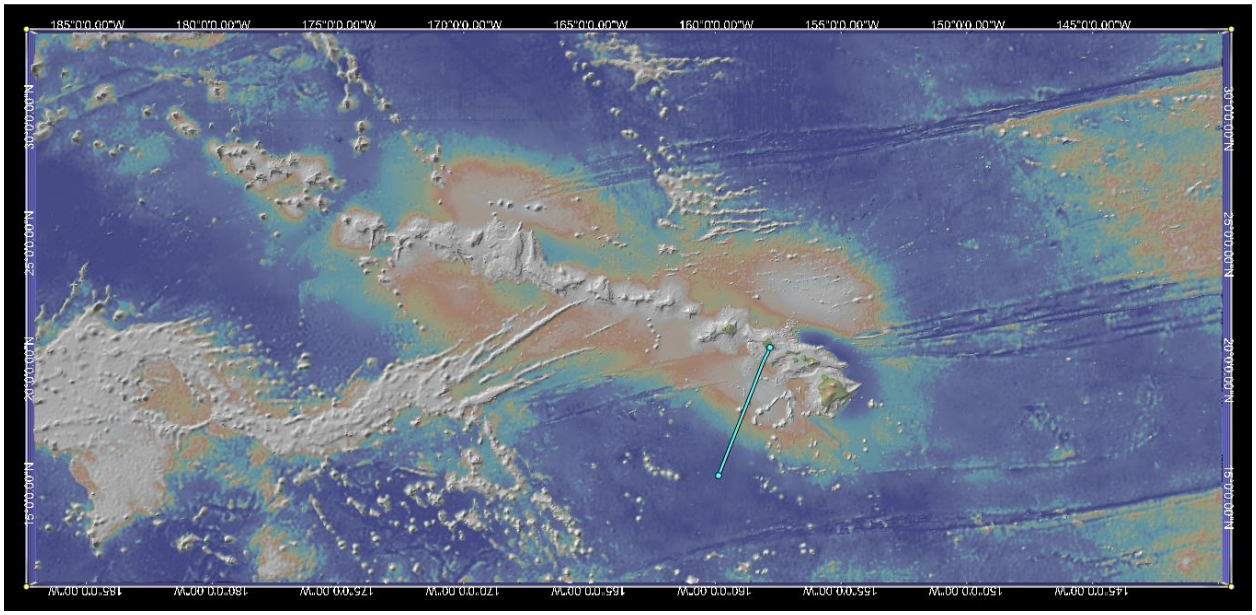

Figure 21g.

8.2 Appendix B

These bathymetric profiles correspond to the topographical profiles represented in Appendix A Figures 10a-g (Figure 11a is the bathymetric profile for Figure 10a etc.). Large spikes seen in the bathymetric profiles, especially seen in Figure 11a and Figure11f are just small basalt deposits on top of the swell. These spikes do not represent the average swell amplitude at that locality.

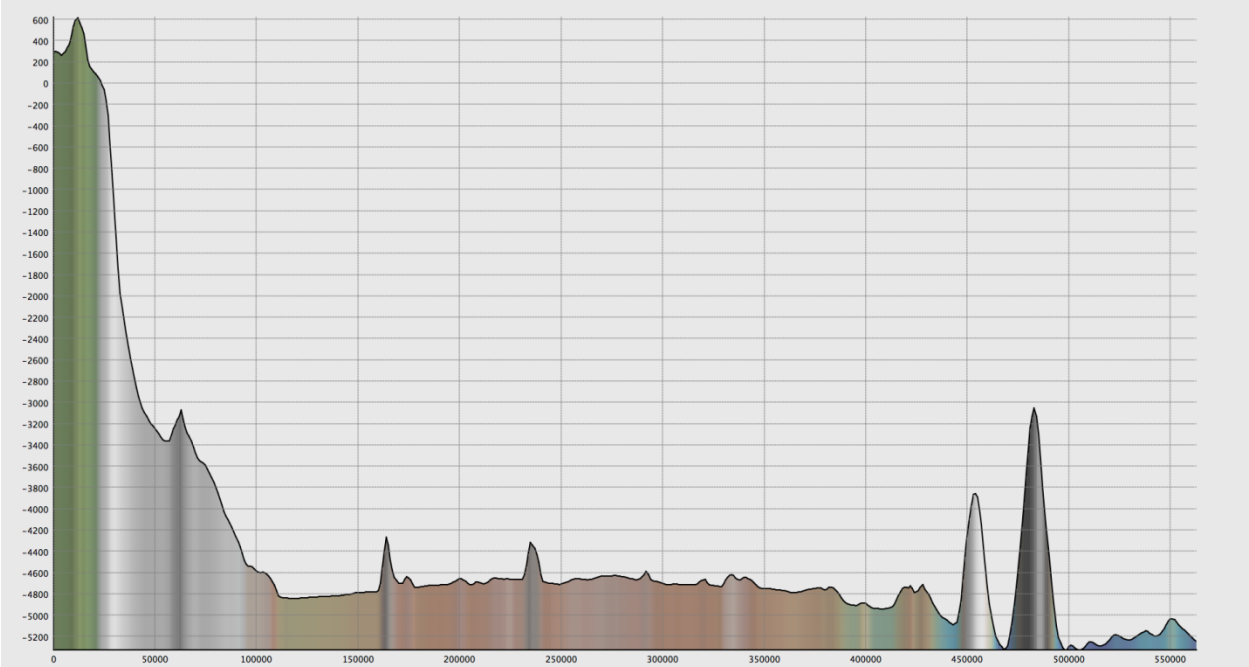

Figure 22a.

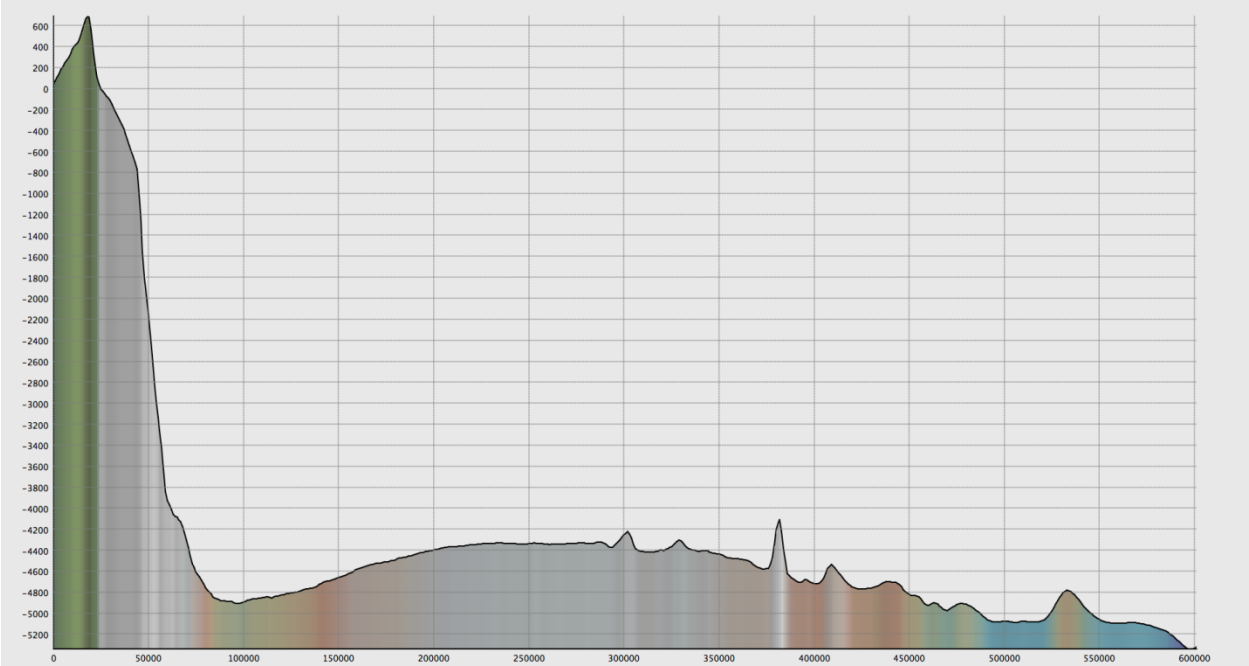

Figure 22b.

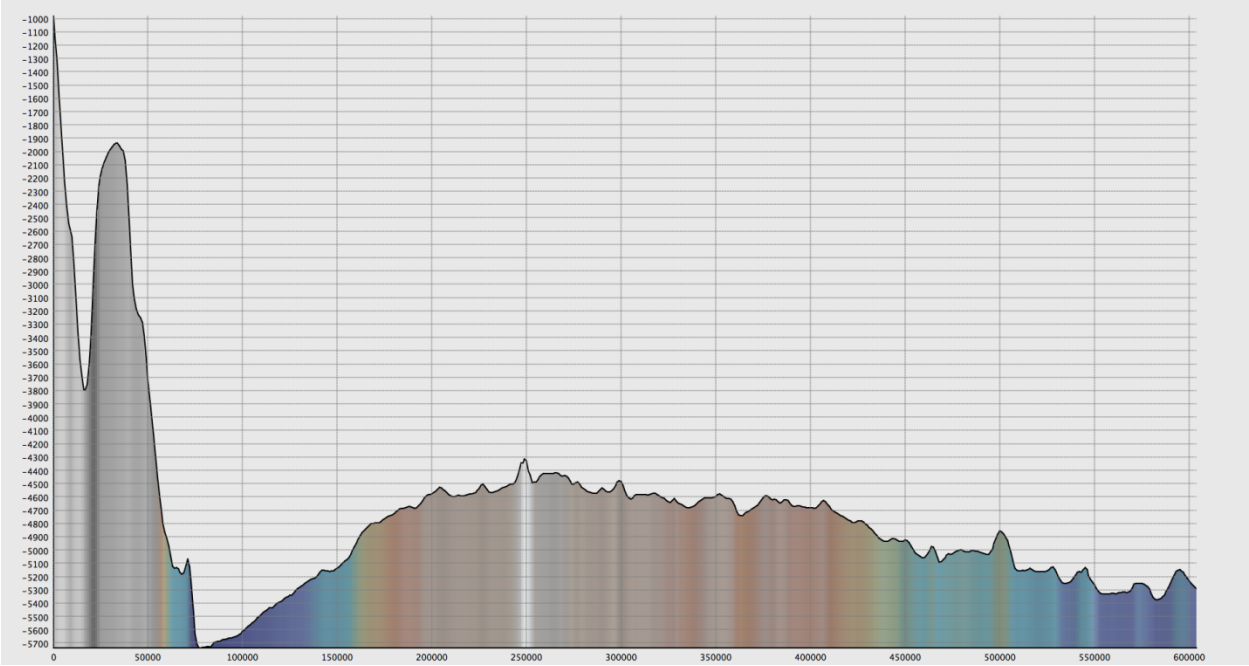

Figure 22c.

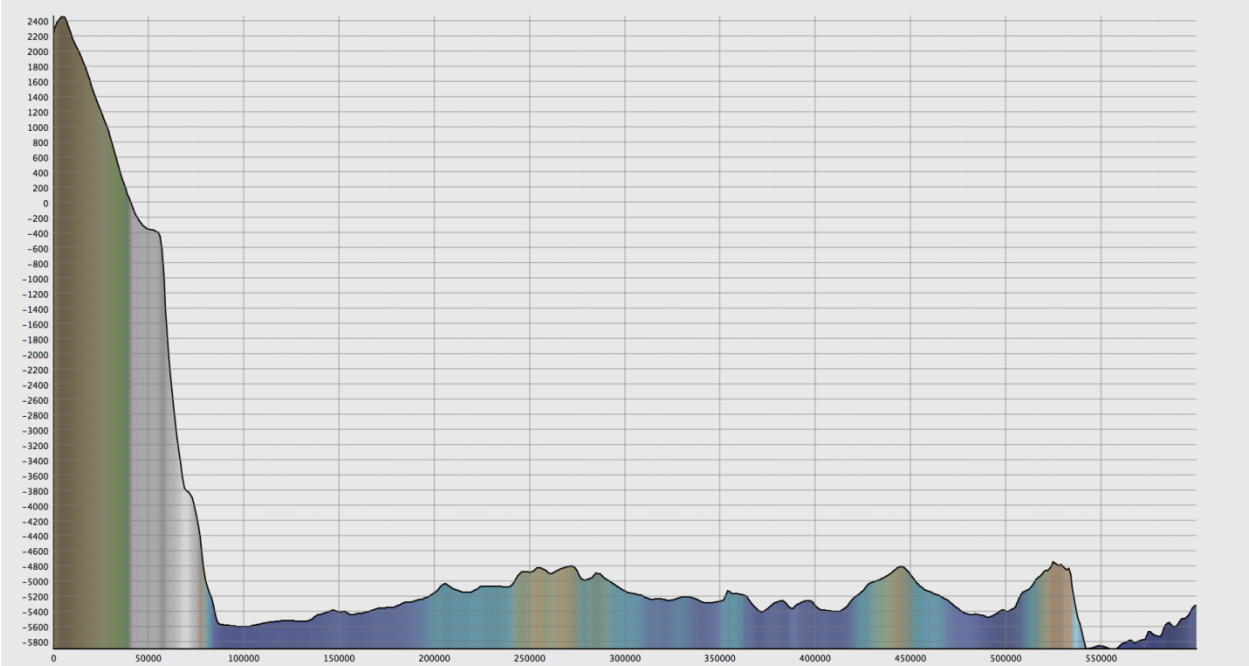

Figure 22d.

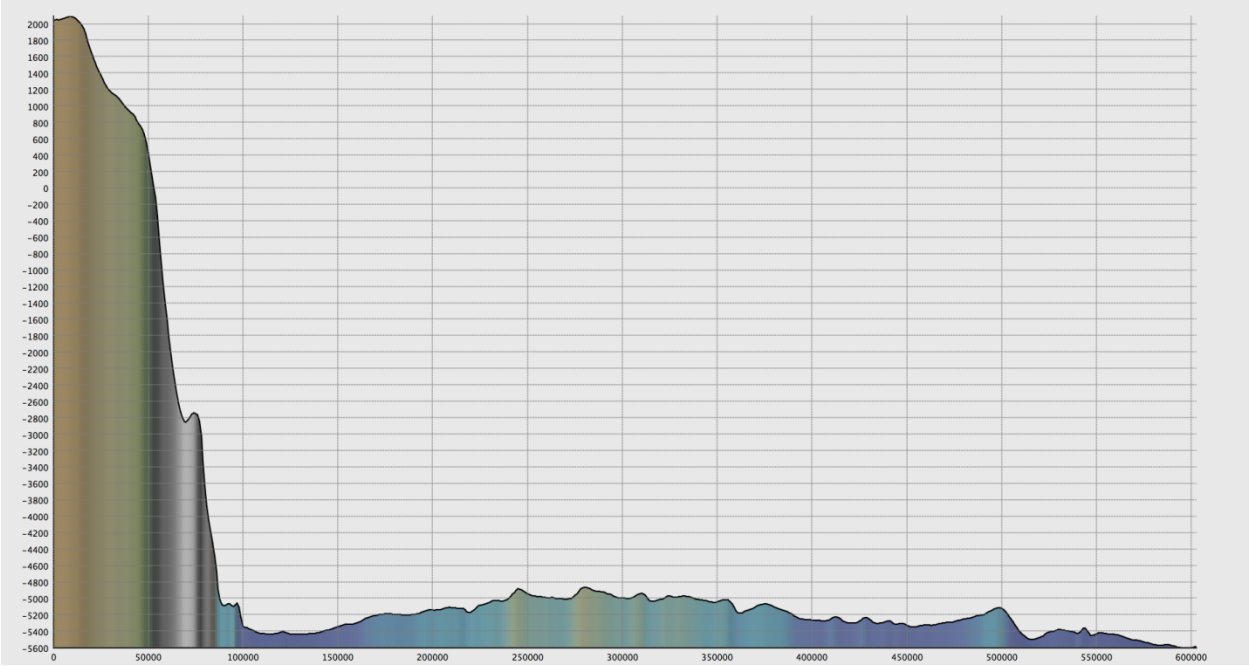

Figure 22e.

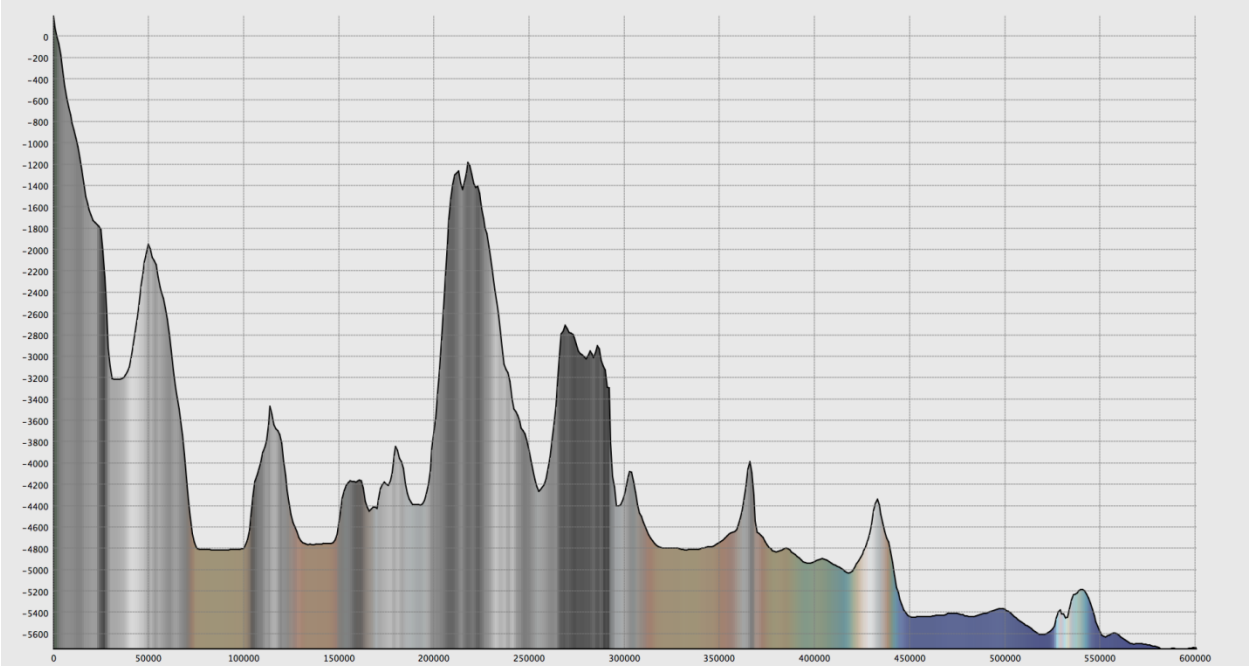

Figure 22f.

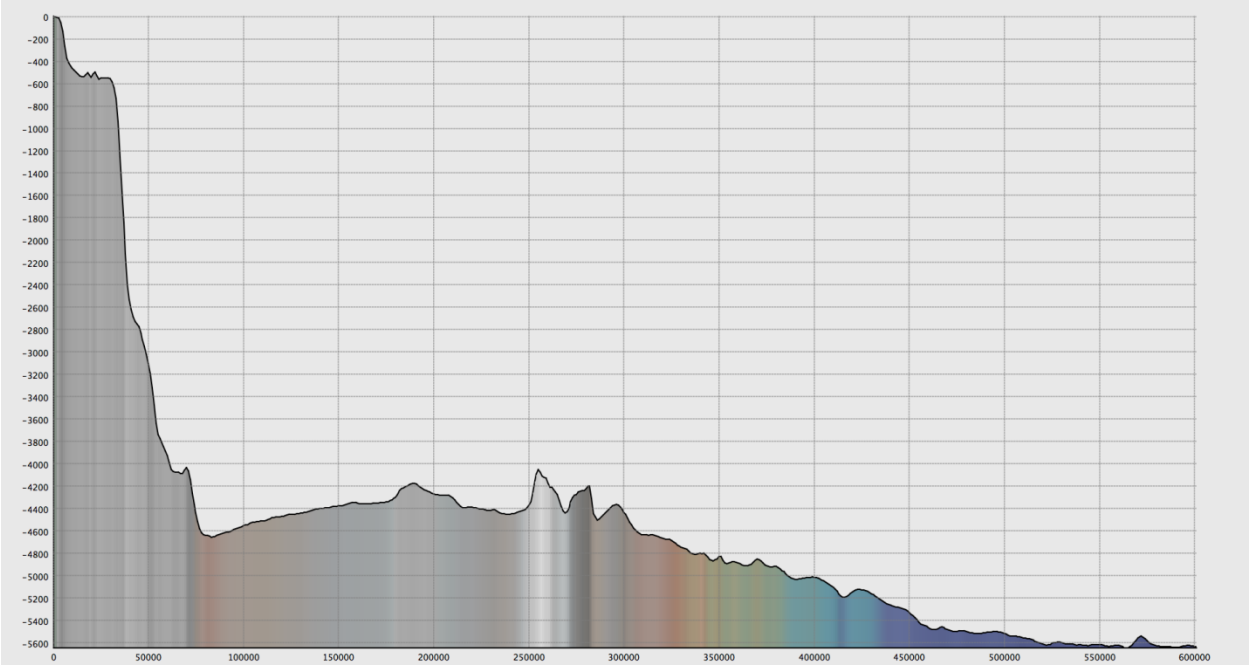

Figure 22g.

8.3 Appendix C

MATLAB code used to define kei. Data provided by Keisan.com.

```
X=[0:0.1:10];
K=[-0.785398163
-0.776850647
-0.758124933
-0.733101912
-0.703800212
-0.671581695
-0.637449495
-0.602175452
-0.566367651
-0.530511122
-0.494994637
-0.460129528
-0.426163604
-0.393291827
-0.361664782
-0.331395562
-0.302565474
-0.275228834
-0.249417069
-0.225142235
-0.202400068
-0.181172644
-0.161430701
-0.143135677
-0.126241488
-0.110696099
-0.096442891
-0.083421858
-0.071570649
-0.060825473
-0.051121884
-0.042395447
-0.034582313
-0.027619697
-0.021446287
-0.016002569
-0.011231096
-0.007076704
-0.003486665
-4.11E-04
```

0.002198399
0.004385818
0.006193613
0.007661269
0.008825624
0.009720919
0.010378865
0.010828725
0.011097399
0.011209526
0.011187587
0.011052008
0.010821278
0.010512056
0.010139286
0.009716307
0.009254964
0.008765716
0.008257737
0.007739025
0.007216492
0.006696059
0.006182749
0.005680767
0.005193579
0.004723992
0.004274219
0.003845946
0.003440398
0.003058385
0.002700365
0.002366486
0.002056629
0.001770454
0.001507429
0.001266868
0.001047959
8.50E-04
6.71E-04
5.12E-04
3.70E-04
2.44E-04
1.34E-04
3.81E-05
-4.45E-05
-1.15E-04

```
-1.74E-04
-2.23E-04
-2.63E-04
-2.95E-04
-3.19E-04
-3.37E-04
-3.49E-04
-3.55E-04
-3.57E-04
-3.56E-04
-3.51E-04
-3.43E-04
-3.33E-04
-3.21E-04
-3.08E-04];
KEI=@(x)interp1(X,K,x);
```

8.4 Appendix D

MATLAB code for Figure 5. Uses the definition of kei provided in Appendix C.

```
clc, clear
DefineKEI;
x=linspace(0,10,100);
B=1;
z=-1.*exp(-sqrt(2).*x/B).*(cos(sqrt(2).*x/B) +sin(sqrt(2).*x/B));
w=(-1/KEI(0)).*KEI(x/B);
% for i=1:100
% w=-1*exp(-sqrt(2)*x(i)/B)*(cos(sqrt(2)*x(i)/B) +sin(sqrt(2)*x(i)/B));
% z(i)=w;
% end
figure(1); clf;
plot(x,z,'linewidth',2)
hold on
plot(x,w,'r','linewidth',2)
legend('lineload','pointload','fontsize',18)
set(gca,'Fontsize',18)
xlabel('Distance x/B','fontsize',24)
ylabel('Displacement w/w(0)','fontsize',24)
```

8.5 Appendix E

I pledge on my honor that I have not given or received any unauthorized help or plagiarized on this assignment.

_____ _____

Christopher Weller Date